UNIVERSITY OF OKLAHOMA

GRADUATE COLLEGE

# IMPACT OF ELEVATED TEMPERATURES ON SOIL TENSILE STRENGTH

A DISSERTATION

SUBMITTED TO THE GRADUATE FACULTY

In partial fulfillment of the requirements for the

Degree of

DOCTOR OF PHILOSOPHY

By

KWESTAN SALIMI

Norman, Oklahoma

2021

Downloaded from SHAREOK. Persistent Handle URL: https://hdl.handle.net/11244/329630

IMPACT OF ELEVATED TEMPERATURES ON SOIL TENSILE STRENGTH

A DISSERTATION APPROVED FOR THE

SCHOOL OF CIVIL ENGINEERING AND ENVIRONMENTAL SCIENCE

BY THE COMMITTEE CONSISTING OF

Dr. Amy B. Cerato, Chair

Dr. Gerald A. Miller

Dr. Kanthasamy K. Muraleetharan

Dr. Kianoosh Hatami

Dr. Andrew Madden

Dr. Farshid Vahedifard

© Copyright by KWESTAN SALIMI 2021

All Rights Reserved.

*Dedicated to the Domestic Violence Survivors*

**Acknowledgments**

I would like to express my sincere gratitude to my advisor, Dr. Amy B. Cerato, for her support and precious guidance for this study. I cannot thank Dr. Cerato enough for her emotional support two years ago during the worst moments of my life. I could have not accomplished none of the works in this dissertation without her gentle heart.

I also gratefully appreciate my outside committee member, Dr. Farshid Vahedifard for his tremendous support, guidance, valuable reviews, and comments that helped improve the quality of this dissertation. I also would like to thank my committee member, Dr. Gerald Miller, a truly great teacher who walked me through the concepts of unsaturated soil mechanics for the first time. I am so grateful to have the opportunity to work with Dr. Miller and learn from his precious advice and comments. I acknowledge Dr. Kanthasamy Muraleetharan, Dr. Kianoosh Hatami and Dr. Megan Elwood Madden for their fantastic teaching, participating on my Ph.D. committee, and for their contribution to my dissertation.

I would like to thank Mr. Michael Schmitz for his technical support and collaboration.

I am grateful to my beloved family for their constant love and encouragement to pursue my dreams.

I would like to express my sincere gratitude to Soheila Haddad and Dr. Baha Jasemnejad for their help and emotional support.

I would also like to thank my friends Rahil Khalili, Vianne Hinsdale, Mehrnoush Nourbakhsh, and Sogol Salary for their help and support.

**Table of Contents**

Acknowledgments.....v

Table of Contents.....vi

List of Tables.....viii

List of Figures.....ix

ABSTRACT.....xii

CHAPTER 1: INTRODUCTION..... 1

1.1 Objectives and Scope of Research..... 3

CHAPTER 2: TENSILE STRENGTH OF COMPACTED CLAYS DURING DESICCATION UNDER ELEVATED TEMPERATURES..... 5

2.1 Introduction..... 5

2.2 Test Apparatus..... 9

2.3 Materials and Procedures..... 13

2.4 Results..... 16

2.4.1 Effect of Temperature on Water Evaporation..... 16

2.4.2 Desiccation Patterns and Tensile Force over Time..... 19

2.4.3 Criteria for Determination of Tensile Strength..... 22

2.4.4 Effect of Temperature on Soil Tensile Strength..... 22

2.4.5 Effect of Initial Water Content on Tensile Strength..... 24

2.5 Discussion ..... 27

CHAPTER 3: A GENERAL MODEL FOR THE UNIAXIAL TENSILE STRENGTH CHARACTERISTIC CURVE OF UNSATURATED SOILS ..... 30

3.1 Introduction ..... 30

3.2 Background ..... 34

3.3 Tensile Strength Characteristic Curve Model ..... 38

3.4 Validation and Comparison ..... 44

CHAPTER 4: A TEMPERATURE-DEPENDENT MODEL FOR TENSILE STRENGTH CHARACTERISTIC CURVE OF UNSATURATED SOILS ..... 62

4.1 Introduction and Background ..... 62

4.2 Tensile Strength Characteristic Curve ..... 65

4.3 Temperature-Dependent Adsorptive Suction Stress ..... 68

4.4 Temperature-Dependent Capillary Suction Stress ..... 71

4.5 Validation and Comparison ..... 73

CHAPTER 5: CONCLUSIONS AND RECOMMENDATIONS ..... 79

5.1 Summary and Conclusion: Tensile Strength of Compacted Clays during Desiccation under Elevated Temperatures ..... 79

5.2 Summary and Conclusions: Tensile Strength of Compacted Clays during Desiccation under Elevated Temperatures ..... 80

5.3 Summary and Conclusion: A General Model for the Uniaxial Tensile Strength Characteristic Curve of Unsaturated Soils ..... 81

5.4 Summary and Conclusion: A Temperature-Dependent Model for Tensile Strength Characteristic Curve of Unsaturated Soils ..... 83

5.5 Recommendations: ..... 84

REFERENCES ..... 85

**List of Tables**

Table 2. 1. Physical and Hydraulic Properties of Chickasha and Idabel Clays (data from Varsei et al., 2016) ..... 14

Table 2. 2. Desiccation Cracking Test Matrix at Different Temperatures ..... 14

Table 3. 1. Basic geotechnical parameters of soils used for model validation and comparison.. 48

Table 3. 2. Parameters of the proposed TSCC model for different soils. ..... 49

Table 3. 3. The coefficient of determination, R2, and the root mean square error (RMSE) of the proposed model and four alternative models in the perdition of laboratory measured tensile strength for different soils ..... 60

Table 4. 1. Measured parameters of soils used for model validation and comparison. ..... 76

Table 4. 2. Input parameters for the SSCC and TSCC ..... 76

**List of Figures**

Figure 2. 1. Crack patterns, constraint conditions, and approximate tensile strain distribution in samples: (a) circular cross section restrained at base; (b) rectangular cross section restrained at base; (c) rectangular cross section restrained at ends (modified after Varsei et al., 2016). ..... 11

Figure 2. 2. (a) Desiccation box; (b) test setup. ..... 12

Figure 2. 3. Variation of water content over time: (a) Chickasha clay at $W_i$ = 18%; (b) Idabel clay at $W_i$ = 24%. ..... 17

Figure 2. 4. Typical process of desiccation cracking: (a) Chickasha clay; and (b) Idabel clay (from Varsei et al. 2016). ..... 20

Figure 2. 5. Variation of tensile force over time for different initial water contents, Chickasha clay at T=20°C (293 K). ..... 21

Figure 2. 6. Variation of tensile force over time for different initial water contents, Idabel clay at T = 20°C (293 K). ..... 21

Figure 2. 7. Variation of tensile force over time, Chickasha clay: $W_i$ =18%..... 23

Figure 2. 8. Variation of tensile force over time, Idabel clay: $W_i$ = 24%. ..... 23

Figure 2. 9. Variation of tensile strength with water content at different temperatures: Chickasha clay. ..... 26

Figure 2. 10. Variation of tensile strength with water content at different temperatures: Idabel clay. ..... 26

Figure 3. 1. a. Uniaxial tensile strength; b. uniaxial tensile strength at failure; c. conceptual illustration of isotropic tensile strength $\boldsymbol{\sigma tia}$ and uniaxial tensile strength $\boldsymbol{\sigma tua}$ based on the concept of suction stress for Mohr-Coulomb criterion failure (modified after Lu et al., 2009). . 40

Figure 3. 2. Conceptual illustration of suction stress curve incorporating both capillarity and adsorption (modified after Zhang and Lu, 2020). ..... 44

Figure 3. 3. Hypothetical stress paths for a desiccation test and for a constant water content tensile strength test ..... 47

Figure 3. 4. SWRC: (a) Esperance sand e=0.82; (b) Perth sand e=0.67; (c) Silica sand e=0.65; (d) Manchester silt e=0.73; (e) Tailings silt e=0.84. ..... 51

Figure 3. 5. SWRC: (a) Idabel clay; (b) Chickasha clay; (c) Nanjing Clay; (d) Plessa clay; (e) Glacial Till clay..... 52

Figure 3. 6. SSCC: (a) Esperance sand e=0.82; (b) Perth sand e=0.67; (c) Silica sand e=0.65; (d) Manchester silt e=0.73; (e) Tailings silt e=0.84. ..... 53

Figure 3. 7. SSCC: (a) Idabel clay; (b) Chickasha clay; (c) Nanjing Clay; (d) Plessa clay; (e) Glacial Till clay. ..... 54

Figure 3. 8. The comparison between tensile strength data with the tensile strength model predictions proposed by this study, Lu et al., (2009), Tang et al. (2015), Varsei et al. (2016), and Yin and Vanapalli (2018) for (a) Esperance sand e=0.82; (b) Perth sand e=0.67; (c) Silica sand e=0.65; (d) Manchester silt e=0.73; (e) Tailings silt e=0.84. ..... 58

Figure 3. 9. The comparison between tensile strength data with the tensile strength model predictions proposed by this study, Lu et al., (2009), Tang et al. (2015), Varsei et al. (2016), and

Yin and Vanapalli (2018) for (a) Idabel clay; (b) Chickasha clay; (c) Nanjing Clay; (d) Plessa clay; (e) Glacial Till clay. ..... 59

Figure 4. 1. Soil water retention curve (SWRC) at different temperatures (a) Idabel Clay; (b) Chickasha Clay. ..... 77

Figure 4. 2. Suction stress characteristic curve (SSCC) at different temperatures: (a) Idabel Clay; (b) Chickasha Clay. ..... 77

Figure 4. 3. Tensile strength characteristic curve (TSCC) at different temperatures: (a) Idabel Clay; (b) Chickasha Clay. ..... 78

**ABSTRACT**

Tensile strength of unsaturated soils is a critical factor controlling the initiation and propagation of desiccation cracks, which can threaten the structural integrity of natural and man-made earthen structures and slopes. Several engineering applications involve unsaturated soils subjected to elevated temperatures (e.g., earthen structure-atmospheric interaction under prolonged droughts, nuclear water disposal, energy piles, ground source heat pumps). While the temperature dependency of desiccation cracking is demonstrated in the literature, critical gaps remain regarding the characterization of the tensile strength under elevated temperatures. The first objective of this study is to experimentally investigate the effect of elevated temperature on the tensile strength of unsaturated clays during desiccation. To accomplish this objective, a novel testing set up that can be used to directly determine soil tensile strength during desiccation was placed in an oven to measure the tensile strength of two compacted clayey soils of medium to high plasticity under different temperatures ranging from 20 °C to 60 °C. The clays are compacted at 95% of their respective maximum dry unit weights over a range of water contents from dry to wet of optimum to investigate the influence of initial water content on tensile strength. The results demonstrated that the tensile strength decreased with increasing temperature. At the optimum water content, a tensile strength reduction of 36% and 27% in the highly plastic clay and the medium plastic clay, respectively, was observed when the temperature increased from 20 °C to 60 °C. Additionally, for the partially saturated condition, the initial water content affected the tensile strength significantly. Temperature-induced changes in key factors contributing to the

tensile strength of unsaturated clays are discussed to provide further insight into tensile strength of clays at elevated temperatures.

It is not always feasible to experimentally determine the tensile strength. Therefore, it is critical to characterize tensile strength analytically to investigate the influence of desiccation and tensile cracks on the structural integrity of natural and man-made earthen structures and slopes. While several models for the prediction of tensile strength of unsaturated soils have been proposed in the literature, critical gaps remain regarding proposing a comprehensive model describing the tensile behavior of all soil types over a wide range of suction. The second objective of this research is to present a general model for the tensile strength characteristic curve (TSCC), which establishes a relationship between the tensile strength versus water content in unsaturated soils. The proposed model is applicable to various soil types ranging from clean sands to silty and clayey soils. Tensile strength is characterized using the suction stress concept and the TSCC model is built upon the concept that changes in tensile strength with water content (or degree of saturation) are primarily dominated by two distinct water retention mechanisms of capillarity and adsorption. Differences in the characteristics of capillary and adsorptive mechanisms and interparticle forces cause dissimilarities in the resultant TSCC in different soil types. Thus, a two-part suction stress characteristic curve (SSCC) was incorporated into the development of the TSCC to separately account for and distinguish interparticle forces and the resultant tensile strength under capillary and adsorptive mechanisms. The model was then validated against laboratory measured tensile strength reported in the literature for ten soils and found to capture the tensile behavior of sandy, silty, and clayey soils well. Compared to several alternative models, the

predictive accuracy of the proposed model was greater, particularly for clayey soils at low water contents (high suction). This superior performance can be attributed to properly accounting for the effect of adsorption mechanism, which is significant in clays.

Desiccation cracks are triggered in unsaturated soils due to drying imposed by natural processes or engineering applications mainly involving elevated temperatures. However, there is no closed-form model in the literature to capture the effect of temperature on tensile strength. The third objective of this research is to present a temperature-dependent model for the tensile strength characteristic curve (TSCC) of unsaturated soils. The model employs the suction stress characteristic curve (SSCC) to represent the uniaxial tensile strength of unsaturated soils at different water contents and temperatures. The model incorporates the effects of temperature into adsorptive and capillary suction stress components. The temperature-dependent adsorptive suction stress is obtained by accounting for thermal induced changes in suction stress at dry state through the Hamaker constant and the density of water. The temperature-dependent form of capillary suction stress is derived by employing temperature-dependent forms of surface tension, contact angle and enthalpy of immersion. Upon comparison, results from the proposed TSCC exhibited a very good agreement against laboratory-measured tensile strength data for two clayey soils tested at different temperatures ranging from 20 to 60 °C. The presented model can improve the analysis of desiccation cracking in unsaturated soils.

## CHAPTER 1: INTRODUCTION

There are several engineering applications in which unsaturated soils are subjected to elevated temperatures and nonisothermal conditions (e.g., McCartney et al., 2019). Such problems include soil-atmosphere interaction under prolonged droughts and heatwaves exacerbated in a changing climate (e.g., Vahedifard et al., 2015, 2016, 2018a; Robinson and Vahedifard, 2016), wildfire-related slope instability and debris flow (Cannon and Gartner, 2005; Abbate et al., 2019), disposal and storage of nuclear waste (e.g., Ma and Hueckel, 1992; Zheng et al., 2015), buried high voltage cables (e.g., Garrido et al., 2003; Salata et al., 2015), shallow geo-energy technologies (e.g., Moradi et al., 2015; Başer et al., 2018), smoldering combustion and remediation (e.g., Ettala et al., 1996; Switzer et al., 2015), and thermally active earthen structures (e.g., Coccia et al., 2013; Stewart et al., 2014).

When the earthen structures are composed of clays soils, desiccation cracks develop on the surface and can extend to several meters below the ground surface (Wang et al., 2018). The presence of cracks in a soil bed adversely alters the hydro-mechanical behavior of the soil during rainfall seasons (e.g., Baker, 1981; Sánchez et al., 2014; Khan et al., 2017; Li et al., 2019). Cracks increase the hydraulic conductivity allowing water to rapidly infiltrate through soil layers, causing loss of suction and potentially, positive pore water pressures, which can degrade the stability of slopes and earthen structures in a variety of geological and geo-environmental settings (e.g., Omidi et al., 1996; Albrecht and Benson, 2001; Nahlawi and Kodikara, 2006; Cheng et al., 2020; Morovatdar et al., 2020a). In addition to an increase in the hydraulic conductivity, desiccation cracks weaken the soil and decrease the soil mass strength significantly (e.g., Morris et al., 1992;

Tang et al., 2015). This modification to the performance of desiccated soils could trigger the initiation of slope failure and cause costly damages to various infrastructure systems including natural and man-made slopes, earth retaining systems, underground structures, pavement and foundations (e.g., Morris et al., 1992; Albrecht and Benson, 2001; Take, 2003; Tang et al., 2010; Zeng et al., 2019; Morovatdar et al., 2020b, and 2020c).

The studies on the temperature dependency of desiccation cracking have shown that larger intact areas of soil remained surrounded by fewer but more contiguous cracks with rise in temperature (Tang et al. 2008), and the evaporation rate and the surface crack ratio increase with increasing temperature (Tang et al. 2008). It is important to better understand the influence of elevated temperatures on the initiation and propagation mechanisms of desiccation cracks and their consequences in order to evaluate the performance of desiccated clays when analyzing different earthen structures and applications in which unsaturated clays are subjected to elevated temperatures. The latter requires a thorough understanding of the impact of elevated temperatures on tensile strength as the main soil property controlling the development of desiccation cracks (e.g., Morris et al., 1992; Peron et al., 2009; Amarasiri et al., 2013; Lachenbruch, 1961; Ayad et al., 1997; Amarasiri and Kodikara, 2011; Kodikara and Costa, 2013; Li et al., 2019). When suction-induced tensile stress exceeds the tensile strength of a clay restrained from shrinkage, desiccation cracks occur on the soil surface (e.g., Tang et al., 2015; Varsei et al., 2016; Li et al., 2019; Zeng et al., 2019).

### 1.1 Objectives and Scope of Research

The main goal of this research is to advance the understanding of unsaturated soils under a changing temperature environment. The objectives of the research are to: (1) To experimentally investigate the effect of elevated temperature on the tensile strength of unsaturated clays during desiccation and provide experimental data, which there is none in the literature, for development and validation purposes of modeling efforts in future studies; (2) To present a general model for the tensile strength characteristic curve (TSCC), which establishes a relationship between the tensile strength versus water content in unsaturated soils ranging from clean sands to silty and clayey soils; (3) To validate the general tensile strength model against laboratory measured tensile strength reported in the literature for sandy, silty, and clayey soils; (4) To present a temperature-dependent model for the tensile strength characteristic curve (TSCC) of unsaturated soils, which can be integrated into analytical and numerical simulations leading to more accurate assessment of desiccation cracking in unsaturated slopes and earthen structures subject to elevated temperatures; (5) To validate the proposed TSCC against laboratory-measured tensile strength data for two clayey soils tested at different temperatures ranging from 20 to 60 °C.

It is believed that the findings of this study can contribute toward more realistic analysis and design of earthen structures subjected to elevated temperatures. To meet the objectives of this study, the following research scope was completed:

- Measured soil tensile strength under non-isothermal conditions using the direct tensile test apparatus developed by Varsei et al. (2016); Carried out a series of direct

tensile tests on two different soils compacted over a range of water contents under elevated temperature ranging from 20 °C to 60 °C.

- Developed a general model for the tensile strength characteristic curve (TSCC), which is applicable to various soil types ranging from clean sands to silty and clayey soils; Included adsorption component of tensile strength separately from capillary component of fine-grained soils which was not included by the previous studies. Compared predications from the proposed model and several alternative models against laboratory measured tensile strength reported in the literature for ten different soils.
- Developed a temperature-dependent model for the uniaxial tensile strength characteristic curve (TSCC) of unsaturated soils, by extending the TSCC model from the previous step for ambient temperature, to non-isothermal conditions. Incorporated the influence of temperature into the parameters contributing to the adsorptive and capillary suction stresses. Validated the accuracy of the proposed TSCC model with laboratory measured tensile strength data for two clayey soils tested at different temperatures ranging from 20 to 60 °C.

# CHAPTER 2: TENSILE STRENGTH OF COMPACTED CLAYS DURING DESICCATION UNDER ELEVATED TEMPERATURES

This chapter has been published as an article in the Geotechnical Testing Journal (Salimi, K., Cerato, A. B., Vahedifard, F., & Miller, G. A. (2021). Tensile Strength of Compacted Clays during Desiccation under Elevated Temperatures. Geotechnical Testing Journal, 44(4). DOI: 10.1520/GTJ20200114). The paper has been reformatted and replicated herein with minor modifications in order to outfit the purposes of this dissertation.

## 2.1 Introduction

Desiccation cracks develop on the surface of, and within slopes and earth structures composed of clayey soils during dry seasons. These cracks form on the soil surface but can extend to several meters below the ground surface (Wang et al., 2018). The presence of cracks in a soil bed adversely alters the hydro-mechanical behavior of the soil during rainfall seasons (e.g., Baker, 1981; Sánchez et al., 2014; Khan et al., 2017; Li et al., 2019). Cracks increase the hydraulic conductivity allowing water to rapidly infiltrate through soil layers, causing loss of suction and potentially, positive pore water pressures, which can degrade the stability of slopes and earthen structures in a variety of geological and geo-environmental settings (e.g., Omidi et al., 1996; Albrecht and Benson, 2001; Nahlawi and Kodikara, 2006; Cheng et al., 2020; Morovatdar et al., 2020a). In addition to an increase in the hydraulic conductivity, desiccation cracks weaken the soil and decrease the soil mass strength significantly (e.g., Morris et al., 1992; Tang et al., 2015). This modification to the performance of desiccated soils could trigger the initiation of slope failure and cause costly damages to various infrastructure systems including natural and man-

made slopes, earth retaining systems, underground structures, and foundations (e.g., Morris et al., 1992; Albrecht and Benson, 2001; Take, 2003; Tang et al., 2010; Zeng et al., 2019; Morovatdar et al., 2020b, and 2020c). Therefore, it is important to better understand the initiation and propagation mechanisms of desiccation cracks and their consequences in order to evaluate the performance of desiccated clays when analyzing different earthen structures. Morris et al. (1992) introduced suction and soil properties such as compression modulus, Poisson's ratio, shear strength, tensile strength, and specific surface energy as the main parameters controlling initiation and propagation of desiccation cracks. For example, it was noted that desiccation cracks primarily develop in fine-grained soils in which high suction develops because of the presence of small pores.

Tensile strength is recognized as the main soil property controlling the development of desiccation cracks (e.g., Morris et al., 1992; Peron et al., 2009; Amarasiri et al., 2013; Lachenbruch, 1961; Ayad et al., 1997; Amarasiri and Kodikara, 2011; Kodikara and Costa, 2013; Li et al., 2019). When suction-induced tensile stress exceeds the tensile strength of a clay restrained from shrinkage, desiccation cracks occur on the soil surface (e.g., Tang et al., 2015; Varsei et al., 2016; Li et al., 2019; Zeng et al., 2019). Different experimental testing procedures have been used to measure the tensile strength of fine-grained unsaturated soils either directly or indirectly. In the indirect techniques, different experiments including the Brazilian tensile test, flexure beam test, double punch test, suction-controlled modified triaxial test, and unconfined penetration test are used to establish correlations between the tensile strength and various parameters of unsaturated soils indirectly (e.g., Ajaz and Parry, 1975; Zeh and Witt, 2005; Ghosh

and Subbarao, 2006; Kim et al., 2007; Lutenegger and Rubin, 2008; Kim et al., 2012; Trabelsi et al., 2012). In the direct methods, however, the tensile strength is measured using uniaxial tensile tests by applying a tensile load to the two ends of a soil specimen (e.g., Ajaz and Parry, 1975; Tang and Graham, 2000; Nahlawi et al., 2004; Lu et al., 2005; Tamrakar et al., 2005; Vesga, 2009; Lakshmikantha et al., 2012; Tang et al., 2015). In both methods, the tests are carried out at constant water content or under constant suction conditions, which means that the evolution of tensile stress with increase in suction during desiccation is ignored. This issue can affect the applicability of the tests results under conditions where tensile stresses develop due to desiccation, even though they provide useful information about tensile strength (e.g., Varsei et al., 2016). To address this issue, Varsei et al. (2016) designed a desiccation test apparatus to measure the tensile strength directly during the desiccation process and considered the soil as a stress path dependent material.

Most of the previous studies on the determination of soil tensile strength are carried out at ambient temperature. However, there are several engineering applications in which unsaturated soils are subjected to elevated temperatures and nonisothermal conditions (e.g., McCartney et al., 2019). Such problems include soil-atmosphere interaction under prolonged droughts and heatwaves exacerbated in a changing climate (e.g., Vahedifard et al., 2015, 2016, 2018a; Robinson and Vahedifard, 2016), wildfire-related slope instability and debris flow (Cannon and Gartner, 2005; Abbate et al., 2019), disposal and storage of nuclear waste (e.g., Ma and Hueckel, 1992; Zheng et al., 2015), buried high voltage cables (e.g., Garrido et al., 2003; Salata et al., 2015), shallow geo-energy technologies (e.g., Moradi et al., 2015; Başer et al., 2018), smoldering

combustion and remediation (e.g., Ettala et al., 1996; Switzer et al., 2015), and thermally active earthen structures (e.g., Coccia et al., 2013; Stewart et al., 2014).

Despite major advances in characterizing the effect of elevated temperatures on various soil properties (e.g., McCartney et al., 2019; Goodman and Vahedifard, 2019; Vahedifard et al., 2020), there is dearth of information in the literature to experimentally investigate and quantify the effect of temperature on the tensile strength of unsaturated soils. Basically, suction-induced tensile stress is mainly due to water loss by evaporation from the surface of the soil layer. The rate of moisture evaporation has a direct influence on the rate of increase in the suction potential, which allows the development of surface tensile stress (e.g., Kayyal, 1996). Tang et al. (2008) showed that larger intact areas of soil remained surrounded by fewer but more contiguous cracks with rise in temperature. In a follow up study, Tang et al. (2010) observed an increase in evaporation rate and the surface crack ratio with increasing temperature. In other words, at a higher temperature, the surface tensile stress will develop at a higher rate and desiccation cracks initiate faster (Tang et al., 2010). While the temperature dependency of desiccation cracking is demonstrated in the literature, major critical gaps still remain regarding the determination of the tensile strength under elevated temperatures.

The main objective of this study is to investigate the effect of elevated temperature on the uniaxial tensile strength of unsaturated compacted clays during desiccation. For this purpose, the direct tensile test apparatus developed by Varsei et al. (2016) is used in order to measure soil tensile strength under non-isothermal conditions. A series of direct tensile tests are carried out

on two different soils compacted over a range of water contents. The effect of elevated temperature ranging from 20 °C to 60 °C on soil tensile strength is then discussed.

### 2.2 Test Apparatus

Varsei et al. (2016) developed a desiccation test apparatus to determine soil tensile strength directly during the natural desiccation process. They designed the desiccation box to reduce the complicated desiccation problem to a simple one-dimensional problem so that desiccation can be studied as an elemental problem resulting in a direct determination of the soil tensile strength. In elemental test procedures, such as a triaxial shear test, stresses and strains are known, and the stress-strain behavior can be directly determined. Before the development of the apparatus by Varsei et al. (2016), previous experimental studies of desiccation cracking (e.g., Miller et al., 1998; Lakshmikantha et al., 2006; Rodríguez et al., 2007; Costa et al., 2013) used samples with different geometries such as circular and rectangular cross sections constrained over the entire base of the samples. For such samples, as illustrated in Figs. 2. 1(a and b), a highly nonlinear distribution of stress and strain results in multiple cracks with random patterns. The interpretation of tensile strength from such sample behavior is highly complicated, requiring sophisticated back analysis. However, as suggested in Fig. 2. 1(c), if a prismatic specimen is constrained at the ends during the desiccation process, uniaxial contraction of the soil takes place and uniform tensile strains and stresses will develop to a large degree near the center of the specimen. Note, the strain distributions presented in Figure 2. 1 are hypothetical and presented

to show how the restriction of soil movements at the boundaries may affect the development of strains, and hence tensile stresses that develop during desiccation.

As shown in Fig. 2. 2(a), Varsei et al. (2016) placed screws in the end walls of the box in order to create a nearly one-dimensional constrained condition during desiccation. In this study, the same desiccation test apparatus designed and developed by Varsei et al. (2016) was used to investigate the effects of elevated temperatures on the tensile strength of unsaturated soils.

The test apparatus is an aluminum box with outside dimensions of 30 cm × 25 cm × 2.54 cm (length × width × height) constructed out of six 1.27 cm thick aluminum plates as shown in Fig. 2. 2(a). The box is built of two halves; one half is fixed, and the other is supported by four roller balls in order to reduce the friction between the box and the surface below it. To monitor the tensile force generated in a soil specimen while drying, two 4.45 kN load cells were attached to the desiccation box where two halves joined. The tension in the soil is transmitted to the load cells through a small gap between the two halves of the box. Therefore, the development of desiccation cracks can be controlled using this test apparatus during the desiccation process, which reasonably simulates the natural process of developing tensile stress with water loss. To apply elevated temperature conditions to the test, the whole testing apparatus except the read-outs was placed in an oven as shown in Fig. 2. 2(b). The read-outs were placed outside the oven to monitor the tensile force periodically. In this study, the soils were exposed to 20 ±1 °C, 40±1 °C, and 60±1 °C drying temperatures. The load cells have an accuracy of ±0.15% over a compensated temperature range of -15 to +65 °C. Following Rohatigi et al. (2006), the authors calculated the volume expansion of the aluminum box when temperature increases from 20 ±1

°C to 40±1 °C and 60±1 °C. It was found that in this range of temperatures, the aluminum coefficient of thermal expansion is low enough that the volume expansion of the aluminum device can be ignored. Therefore, the device and load cells work well under the desired tested temperatures in this study. Additionally, to monitor the water loss, a digital scale with a capacity of 30 kg, readability of 0.1 g, and accuracy of ±0.5 g is used for the experiments.

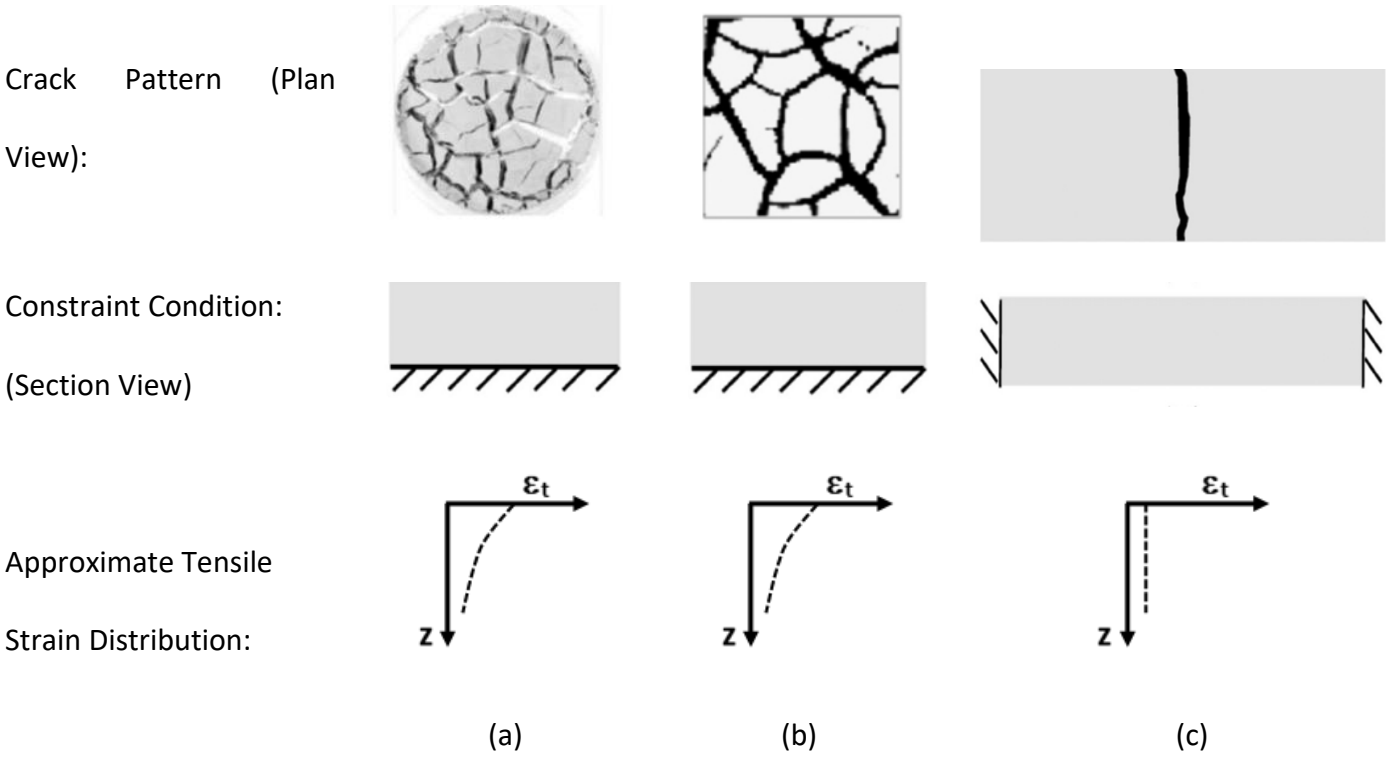
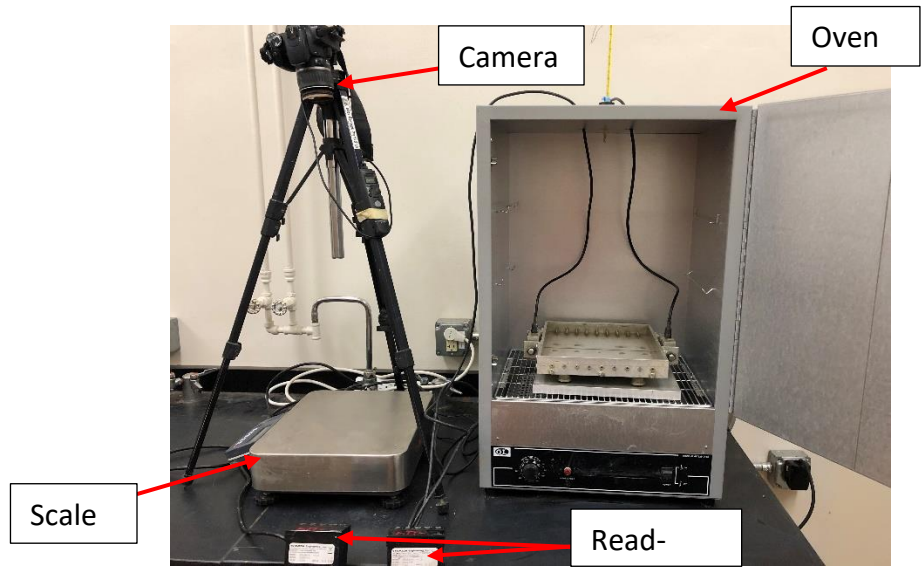
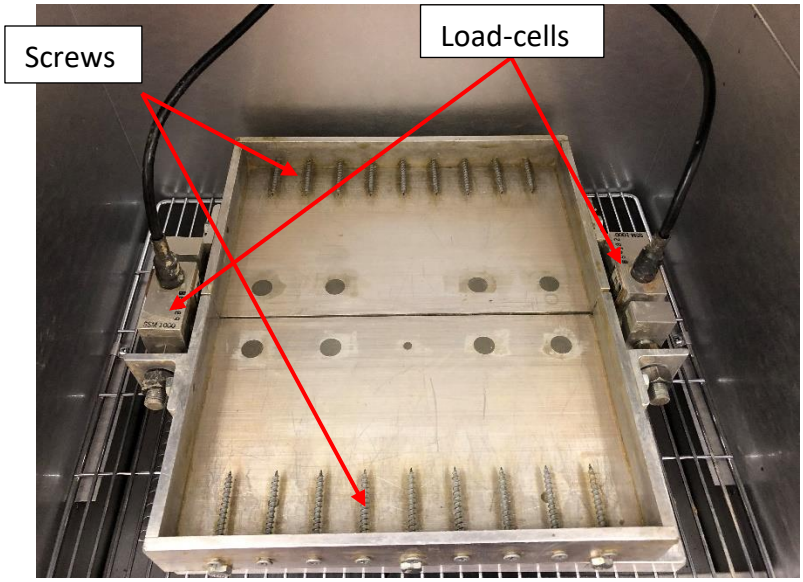



**Figure 2. 1. Crack patterns, constraint conditions, and approximate tensile strain distribution in samples: (a) circular cross section restrained at base; (b) rectangular cross section restrained at base; (c) rectangular cross section restrained at ends (modified after Varsei et al., 2016).**




(a)




(b)

**Figure 2. 2. (a) Desiccation box; (b) test setup.**

## 2.3 Materials and Procedures

The two fine-grained soils used for testing are Chickasha and Idabel clays found at two different sites located in Oklahoma. These sites were chosen for this study because they have been exposed to desiccation cracks and shallow slope failures over time. Selected properties of these clays were obtained from Varsei et al. (2016) and summarized in Table 2. 1. According to the Unified Soil Classification System (USCS), Chickasha and Idabel clays are classified as lean clay (CL) and highly plastic clay (CH), respectively. Idabel clay is known to be highly expansive with significant shrink-swell potential. Table 2. 1 also shows the fitting parameters of the van Genuchten's soil water retention curve (SWRC) model (van Genuchten, 1980) for these two clays. The SWCCs was determined following the method used by Varsei et al. (2016).

**Table 2. 1. Physical and Hydraulic Properties of Chickasha and Idabel Clays (data from Varsei et al., 2016)**

| Property | Chickasha clay | Idabel clay |
|---|---|---|
| Liquid limit (%) | 38 | 72 |
| Plastic Limit (%) | 20 | 26 |
| Plasticity index | 18 | 46 |
| Specific gravity | 2.75 | 2.78 |
| Gravel (%) | 0 | 0 |
| Sand (%) | 10.6 | 3.5 |
| Silt (%) | 49.4 | 16.9 |
| Clay (%) | 40 | 79.6 |
| Maximum dry unit weight ($kN/m^3$) | 17.3 | 15.2 |
| Optimum water content (%) | 18 | 24 |
| van Genuchten SWRC parameter n | 1.4 | 1.35 |
| van Genuchten SWRC parameter α (1/kPa) | 0.032 | 0.013 |

**Table 2. 2. Desiccation Cracking Test Matrix at Different Temperatures**

| Soil type | Target drying temperature (°C) | Target initial water content ($W_i$ %) |
|---|---|---|
| Chickasha clay | 20, 40, and 60 | 12, 15, 18, and 22 |
| Idabel clay | 20, 40, and 60 | 18, 20, 22, 24, 30, and 34 |

The tested soils were first sieved through a No. 4 US standard sieve and wetted to achieve a range of water contents around their optimum water contents. The samples were kept in a humid room for at least two days to allow water to be more uniformly distributed throughout the soil. Then, the soil was uniformly compacted in the desiccation box in one layer to a thickness of 1.5 cm. The soils were compacted at 95% of their respective maximum dry unit weights over a range of water contents from dry to wet of optimum to investigate the influence of initial water content on tensile strength. The initial water contents are referred as $W_i$ in the rest of this paper. To minimize the friction between the soil and base of the box, Teflon sheets were used.

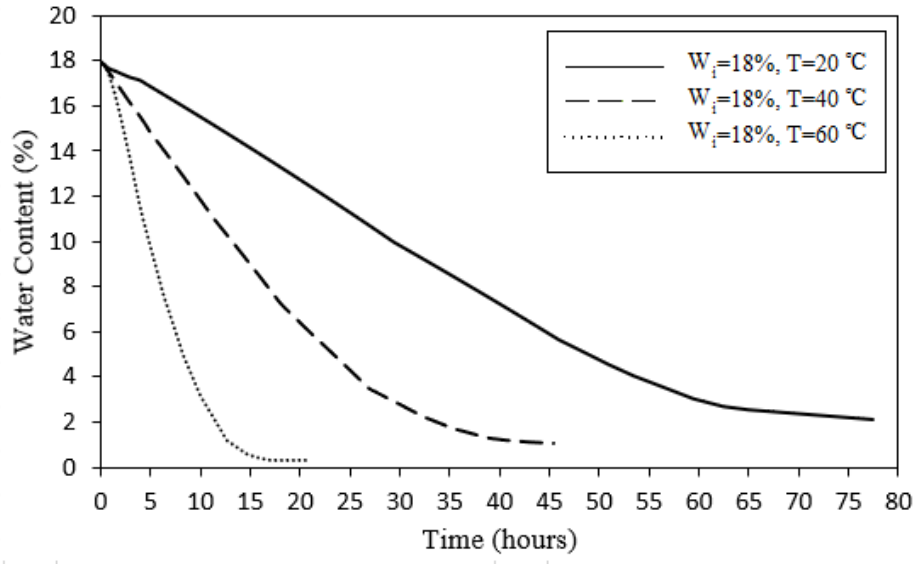
To study the effects of elevated temperatures on the tensile strength, identical specimens were prepared and exposed to 20 ±1 °C, 40±1 °C, and 60±1 °C drying temperatures with the use of an oven. Due to the limitation of the scale exposed to high temperatures (40 °C and 60 °C), the desiccation box must be removed from the oven to monitor water content periodically. In order to keep the temperature of the specimen constant, the box weight measurement process was performed in less than 15 seconds so that the environmental temperature variation between oven and room does not change the specimen temperature. In this case, the drying rate was considered the same during the measurement of the tensile strength and the water loss. A camera and an intervalometer are used for time-lapse photography of read-outs placed outside the oven to monitor tensile force under different temperatures.

Table 2. 2 shows the testing matrix used for this study. Repeated samples were tested to confirm the accuracy and repeatability of the testing setup and procedure.

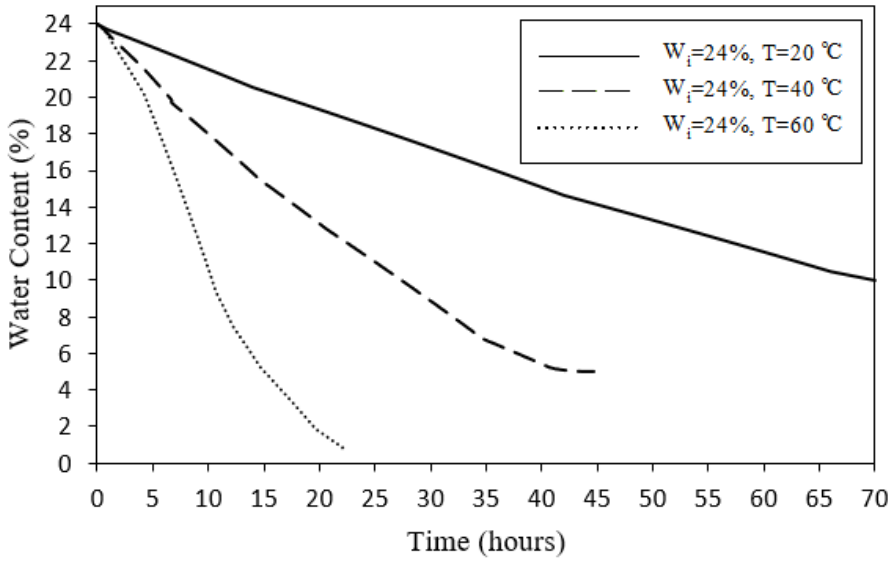
## 2.4 Results

### 2.4.1 Effect of Temperature on Water Evaporation

Figs. 2. 3 (a and b) show the water content changes upon desiccation at various drying temperatures of 20 °C, 40 °C and 60 °C for Chickasha and Idabel clays, respectively, compacted at their optimum water contents ($W_i$ =18% for Chickasha clay and $W_i$=24% for Idabel clay). At first, the water content decreased linearly and then approached a residual moisture condition in both soils. It took longer for samples exposed to 20 °C to dry out compared with the identical samples exposed to 40 °C and 60 °C. For example, as shown in Fig. 2. 3(a), under 20 °C, Chickasha samples required more than 60 hours to approach the residual moisture condition, while this value reduced to approximately 35 and 15 hours for identical Chickasha samples exposed to 40 °C and 60 °C, respectively. The same observation is noted for Idabel samples as shown in Fig. 2. 3(b). However, Idabel samples needed a longer time to reach a residual moisture condition compared to Chickasha samples due to being highly plastic and having more tendency to retain water. This observation regarding the dependency of soil evaporation rate and duration upon different drying temperatures agrees with that made by Tang et al. (2010) who conducted desiccation tests on identical slurry samples exposed to 22 °C, 60 °C, and 105 °C temperatures.




(a)




(b)

**Figure 2. 3. Variation of water content over time: (a) Chickasha clay at $W_i$ = 18%; (b) Idabel clay at $W_i$ = 24%.**

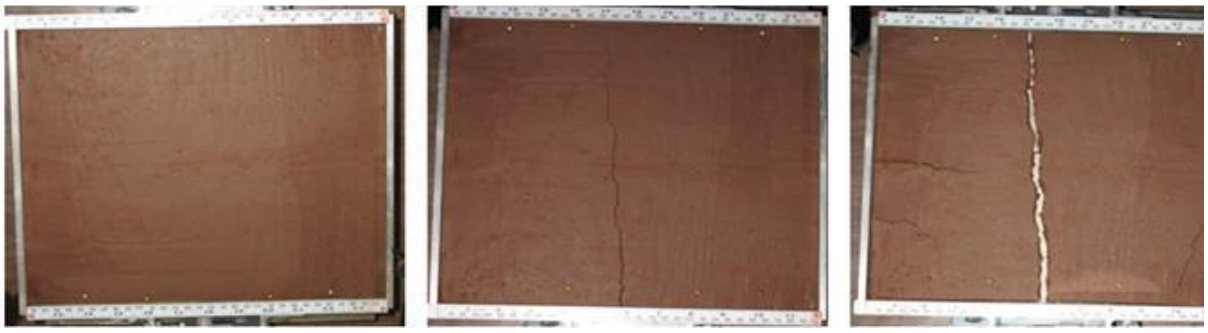
Temperature, relative humidity, wind velocity, solar radiation, soil suction, salt concentration, soil pore size and layer thickness are among factors influencing the rate and duration of the water loss from the soil surfaces (e.g., Kayyal, 1996; Cui et al., 2005; Tang and Cui, 2005; Prat et al., 2006; Rodríguez et al., 2007; Tang et al., 2010). For example, with an increase in temperature, the water molecule motion velocity and kinetic energy increase while viscosity, the interfacial tension of water and water retention capacity decrease (Tang and Cui, 2005; Tang et al., 2010). Higher drying temperatures help water molecules to escape faster to the atmosphere resulting in a higher water evaporation rate. In addition to the faster water molecules motion, higher temperatures result in lower relative humidity across the soil-air interface in accordance with Kelvin's temperature scale. Therefore, relative humidity gradient or water evaporation rate from the soil surface increases in order to keep vapor pressure across the upper air layer and soil interface balanced at the elevated temperatures (Tang et al., 2010).

As shown in Fig. 2. 3(a), the residual moisture contents at the end of testing were lower at higher temperatures. At the end of testing for the Chickasha samples, the water content was approximately 4% at 20 °C, 1.5% at 40 °C and 0.5% at 60 °C. A similar trend can be seen for the Idabel samples. At these low water contents, the amount of water held by the clay particles is a function of the physico-chemical interactions in the diffuse double layers, which depend on temperature.

### 2.4.2 Desiccation Patterns and Tensile Force over Time

Figs. 2. 4(a and b) show that, as expected, a nearly linear crack initiated and propagated across the width of the desiccation box in Chickasha and Idabel clay samples. Placing screws at boundaries restricted the shrinkage of the clay bed as it dried, causing nearly uniaxial tensile stresses to develop at the middle of the specimen in the longitudinal direction. When these stresses reach a limiting value, i.e. the tensile strength, a crack developed across the width of the box nearly perpendicular to the direction of the major principal tensile stress. A similar pattern of crack development was observed for all specimens.

Figs. 2. 5 and 6 depict the variation of tensile force versus time for Chickasha and Idabel clays, respectively at 20 °C. Upon desiccation with an increase in suction, the tensile force first increased up to a peak value before showing a loss in tensile force indicating an initiated desiccation crack. After the crack initiation, the tensile force decreased. Cracks opened at different times depending on the initial water contents. For example, cracks opened faster when clays were compacted at dry of optimum water content in comparison to the wet of optimum water content.



(a)



(b)

**Figure 2. 4. Typical process of desiccation cracking: (a) Chickasha clay; and (b) Idabel clay (from Varsei et al. 2016).**

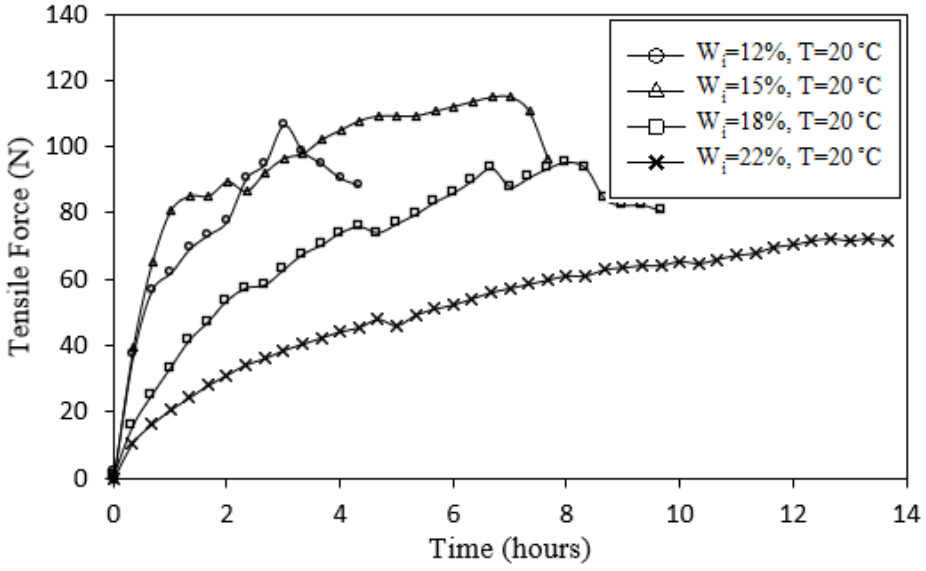



**Figure 2. 5. Variation of tensile force over time for different initial water contents, Chickasha clay at T=20°C (293 K).**

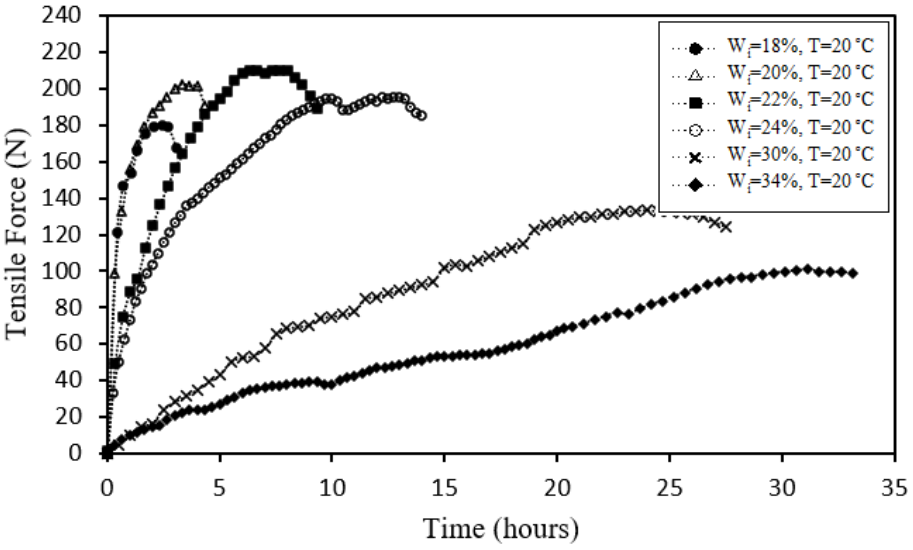



**Figure 2. 6. Variation of tensile force over time for different initial water contents, Idabel clay at T = 20°C (293 K).**

### 2.4.3 Criteria for Determination of Tensile Strength

In this study, it is assumed that the peak value or maximum tensile force occurs right before the onset of the desiccation crack (failure). In other words, there is no crack in the soil body before the failure when the maximum tensile force is recorded. Therefore, if the maximum load is carried by the non-cracked cross-sectional area of the soil bed, one can divide the maximum tensile force by the full cross-sectional area of the specimen in order to calculate the maximum tensile stress that soil can resist during the desiccation process. The initial cross-sectional area of the soil bed is taken as the non-cracked cross-sectional area of the soil specimen because the changes in thickness and lateral shrinkage are insignificant at this stage and can be ignored. Therefore, soil tensile strength equals the calculated maximum tensile stress the soil can resist before failure.

### 2.4.4 Effect of Temperature on Soil Tensile Strength

The main purpose of this research was to investigate the influence of elevated temperatures on the development of the tensile strength of fine-grained soils. Therefore, identical Chickasha and Idabel specimens were prepared and tested under various drying temperatures of 20 °C, 40 °C, and 60 °C. Figs. 2. (7 and 8) show the typical desiccation curves obtained for Chickasha and Idabel specimens compacted at 18% and 24%, respectively. A reduction in peak tensile force for Chickasha and Idabel specimens was observed when drying temperature increased from 20 °C to 40 °C, and 60 °C. For example, for Chickasha clay, the maximum tensile force of 94 N reduced to 69 N when applied temperature increased from 20 °C to 60 °C. This value decreased from 193.5 N to 125 N for Idabel clay.

Figs. 2. (9 and 10) show the variation of tensile strength with water content at different temperatures for Chickasha clay and Idabel clay, respectively. The tensile strength decreased with the increase in drying temperature for both Chickasha and Idabel clays. For example, 24% and 34% reductions in the maximum tensile strength for Chickasha and Idabel clays were observed, respectively, with an increase in drying temperature from 20 °C to 60 °C (Figs. 2. (9 and 10)).

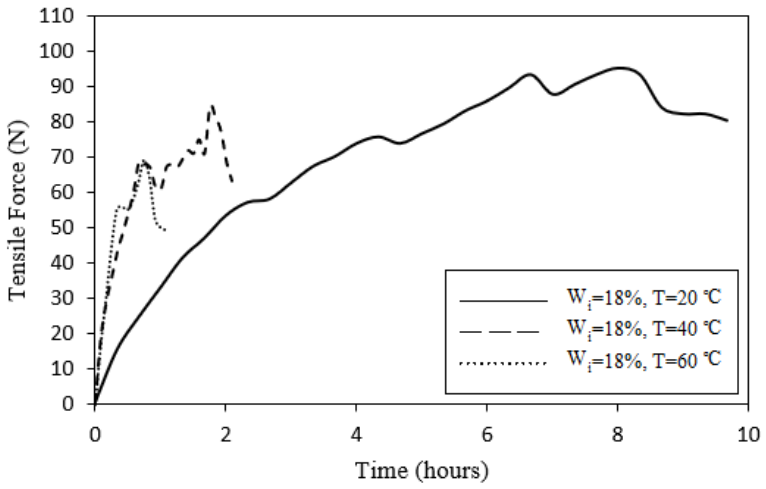



**Figure 2. 7. Variation of tensile force over time, Chickasha clay: $W_i$ =18%.**

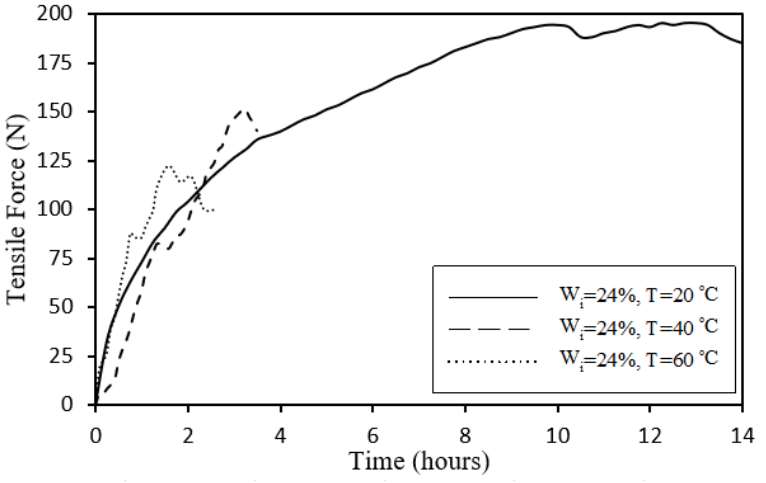



**Figure 2. 8. Variation of tensile force over time, Idabel clay: $W_i$ = 24%.**

### 2.4.5 Effect of Initial Water Content on Tensile Strength

Figs. 2. (9 and 10) indicate that the water content at which the soil specimen is initially compacted influences the development of the tensile strength. This observation is consistent with that reported in the literature (Tang et al., 2015; Varsei et al., 2016). With the increase in the initial water content, the tensile strength increased up to a peak value and then decreased with further increases in the water content. For example, under 20 °C drying temperature, the tensile strength of Chickasha clay increased from 28 kPa to 30.0 kPa with an increase in the initial water content from 12% to 15%. With further increase in the initial water content to 22%, the tensile strength reduced to 18.9 kPa. Under the same drying temperature, an increase in the tensile strength of Idabel clay from 47 kPa to 55 kPa was observed when the initial water content increased from 18% to 22% (Fig. 2. 10). The tensile strength then decreased to 26 kPa for Idabel specimen compacted at higher initial water content of 36%. It can be concluded that with increase in the compaction water content at first, there is a growing trend in the tensile strength of fine-grained soils. Then, a downward trend in tensile strength is observed with further increases in the water content.

Similar trends in the variation of the tensile strength versus the initial water content were observed for specimens while desiccating at temperatures of 40 °C and 60 °C, as was observed for 20 °C drying temperature (Figs. 2. (9 and 10)). This means that at each drying temperature, the soil tensile strength increased up to a peak value with the addition of initial water content. After this point, a reduction in tensile strength was observed with further increase in initial water content.

Moreover, greater tensile strength was developed for Idabel clay compared with Chickasha clay because Idabel clay is highly plastic and has a higher plasticity index and higher capillary forces. This means that the cohesion between particles is greater in Idabel clay resulting in greater development of the tensile strength compared with Chickasha clay, which agrees with the observation reported in several previous studies (e.g., Al-Hussaini and Townsend, 1974; Fang and Fernandez, 1981; Barzegar et al., 1995; Kim and Hwang, 2003; Tamrakar et al., 2005; Kim et al., 2012; Varsai et al., 2016).

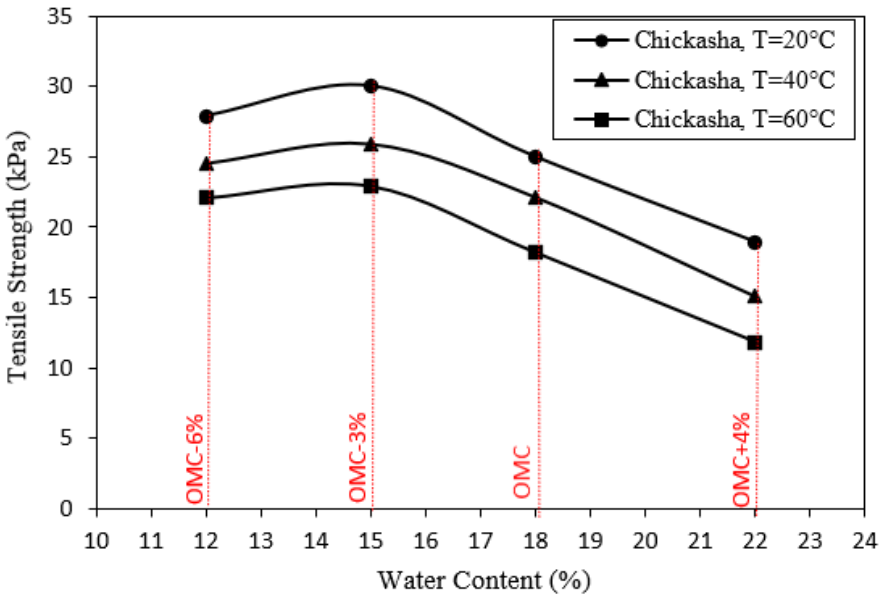



**Figure 2. 9. Variation of tensile strength with water content at different temperatures: Chickasha clay.**

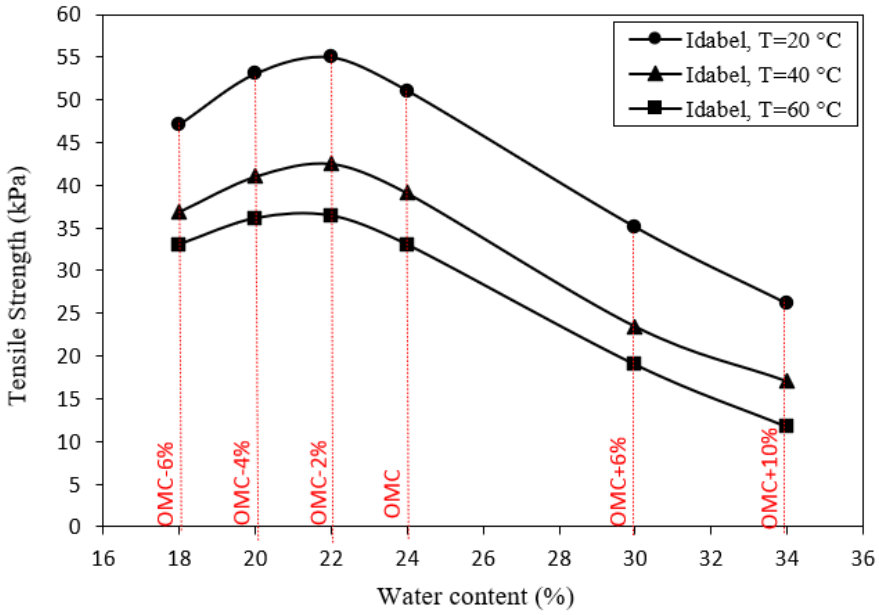



**Figure 2. 10. Variation of tensile strength with water content at different temperatures: Idabel clay.**

## 2.5 Discussion

As illustrated in the result section, temperature affects the development of tensile strength. Increasing temperature changes the mechanisms attributed to the soil cohesion and the resultant tensile strength. Depending on different factors such as soil type, soil mineralogy, range of temperature, range of suction, water content, etc., elevated temperatures can change surface tension of the pore water, soil-water contact angle, soil fabric, water absorption potential, and pore size distribution of soils (e.g., Grant and Salehzadeh, 1996; Romero et al., 2003; Villar and Lloret 2004; Wan et al. , 2015). Previous studies on the influence of elevated temperatures on water retention capacity of soils revealed that soil water content can change the mechanisms by which temperature affects the water retention capacity (Romero et al., 2001, 2003; Villar and Lloret, 2004; Villar et al., 2005; Schneider and Goss, 2011; Vahedifard et al., 2018b, 2019). Therefore, it is expected that the mechanisms by which temperature affects the development of soil tensile strength is also affected by a soil's varying initial water content. For instance, for lower water contents, most of the water is trapped in intra-aggregate pores (micropores) and clayey soil particles are attracted to each other through van der Waals forces along with forces coming from electrostatic repulsion due to surface charges on particles. van der Waals forces are due to electronic fluctuations, and do not depend on temperature; or at least only weakly depend on temperature. However, changing temperature alters the charge on the particles causing the electrical double-layer repulsion forces between platy clay particles to be weakened (Romero et al., 2001; Villar and Lloret, 2004; Villar et al., 2005). Therefore, elevated temperatures decrease the attractive forces between soil particles resulting in less cohesion between them and less

resultant soil tensile strength (Vahedifard et al., 2019). For higher water contents, however, water is trapped between inter-aggregate pores (macropores) and capillary forces create apparent cohesion between soil particles. At this level, soil tensile strength decreases because at elevated temperatures, the apparent cohesion between particles has been weakened through reducing surface tension, expanding trapped air bubbles, isolating water packets and changing the quantity of solute (Romero et al., 2001, 2003; Schneider and Goss, 2011).

Another governing factor in the development of tensile strength was shown to be initial water content. Based on previous work, it is expected that tensile strength should increase as degree of saturation decreases, or as soil suction increases (Towner 1987; Morris et al. 1992; Tang and Graham 2000; Ávila 2004; Nahlawi et al. 2004; Wang et al. 2007). However, as depicted in Figs. 2. (9 and 10), along with the results presented by Tang et al. (2015) and Varsei et al. (2016) show that, in addition to the soil suction, the structure of clays is another factor influencing the development of the suction-induced apparent cohesion and tensile strength of compacted clayey soils. Initial compaction water content can strongly change the arrangement and structural distribution of the fine-grained particles (Tang et al., 2015; Varsei et al., 2016). As a result, the evolution of interparticle forces as a reflection of the pore size distribution of soil particles (Santamarina 2003) are affected by the initial compaction water content. Therefore, considering the influence of water content on the arrangement of the fine-grained particles and the resultant interparticle forces, one can attribute the development of tensile strength to the initial water content in fine-grained soils (Tang et al., 2015; Varsei et al., 2016). When soils are compacted at dry of optimum moisture content, water is trapped between aggregates, which forms water-

bridges in the contact points. The capillary bonding force developed from the water-bridges then results in higher apparent cohesion even though the soil suction decreases. In fact, there are enough inter-aggregates pores in a soil specimen to increase the capillary bonding force and the resultant soil tensile strength with further addition of water. In the current study, in both clays, the tensile strength increased up to a peak value, corresponding to $W_i$=OMC-2%, indicating the full possible development of the water-bridges in the contact points and the resultant capillary bonding force (Figs. 2. (9 and 10)). After this, further addition of water to the soil changed the soil structure to a more aggregate-dispersed structure with less inter-aggregate pores resulting in a reduction in the capillary-induced tensile strength. Further increase of water content increased disconnected water-bridges and decreased the size and number of inter-aggregates pores in soil specimens. Therefore, with further addition of water, the state of water gradually transformed from the disconnected water-bridges to a more connected water state, and suction-induced tensile strength from capillary bonding force between aggregates decreased.

Findings of this research clearly demonstrate the temperature dependency of tensile strength in unsaturated soils. However, the existing closed-from models for tensile strength do not account for the effect of temperature. This highlights the need to develop a temperature-dependent model for tensile strength of unsaturated soils by incorporating the effects of temperature into key contributing factors. The experimental test results presented in the current study provide invaluable data for development and validation purposes of modeling efforts in future studies. If developed, such closed-from model can be integrated into analytical and numerical simulations, leading to more accurate assessment of desiccation cracking in unsaturated slopes and earthen structures subject to elevated temperatures.

# CHAPTER 3: A GENERAL MODEL FOR THE UNIAXIAL TENSILE STRENGTH CHARACTERISTIC CURVE OF UNSATURATED SOILS

This chapter has been accepted to publish as an article in the Journal of Geotechnical and Geoenvironmental Engineering (Salimi, K., Cerato, A.B., Vahedifard, F. and Miller, G.A. (2021). A General Model for Tensile Strength Characteristic Curve of Unsaturated Soils. ASCE JGGE. 10.1061/(ASCE)GT.1943-5606.0002567). The paper has been reformatted and replicated herein with minor modifications in order to outfit the purposes of this dissertation.

## 3.1 Introduction

The existence of tensile cracks in soils increases the hydraulic conductivity (e.g., Omidi et al. 1996; Albrecht and Benson 2001; Cheng et al. 2020) and reduces the shear strength (e.g., Morris et al. 1992; Tang et al. 2015), which can lead to major damage and eventually failure in slopes and earthen structures (Abdollahi et al. 2021). Previous studies have mainly used tensile stress failure criteria (e.g., Morris et al. 1992; Kodikara and Choi 2006; Peron et al. 2009; Amarasiri and Kodikara 2013) or fracture mechanics theories (e.g., Lachenbruch 1961; Konrad and Ayad 1997; Amarasiri et al. 2011; Kodikara and Costa 2013; Hueckel et al. 2014) to describe the formation and propagation of tensile cracks and constitutive behavior of a cracked soil. In both theories, tensile strength is recognized as the main soil property controlling the development of tensile cracks in soils (e.g., Morris et al. 1992; Kodikara and Choi 2006; Peron et al. 2009; Amarasiri and Kodikara 2013; Lachenbruch 1961; Ayad et al. 1997; Amarasiri et al. 2011; Kodikara and Costa 2013; Li et al. 2019) and thus, is used as a key input parameter to develop analytical and numerical models.

Tensile strength develops when the interparticle bonding forces along the failure plane reduce to zero. Therefore, it is necessary to characterize these bonding forces to better explain the development of tensile strength and the mechanical behavior of unsaturated soils (Ingles 1962; Santamarina 2003). Variation in degree of saturation in unsaturated soils changes the ability of soils to attract water (soil-water interactions), and the resultant interparticle forces (Santamarina 2003). Over a different range of suction, changes in soil-water interaction are caused by different governing physical mechanisms (called capillarity and adsorption), which do not directly depend on each other and function separately (Orr et al. 1975). When a saturated soil mass begins to dry, the state of water in the soil varies from capillary water to adsorptive and tightly adsorptive water (Vanapalli et al. 1996; Tuller et al. 1999). In a capillary regime, the soil particle surface is coated with a thick water film (free water), and the tendency of soil particles to be solvated into water creates tension on the mineral surface acting on the air-water film interface and holding liquid in pore corners (creating a curved air-water interface in soil pores) (e.g., Ingles 1962; Fredlund and Morgenstern 1977). This surface tension transmits onto the soil skeleton creating an interparticle bonding force called capillary force (Santamarina 2003). In other words, “capillary force,” underlying the capillary soil-water interaction, refers to interparticle or skeleton force. Capillary pressure is defined by the difference in pore-air and pore-water pressures. The capillary pressure definition is commonly considered to be the same as matric suction. However, several studies (Lu and Khorshidi 2015, Zhang and Lu 2019) have shown that this definition of matric suction is valid only when the local pressure variation due to the existence of adsorptive water is insignificant. While matric suction or capillary pressure may

be the same in two soils, the resulting capillary forces can be dramatically different. The magnitude and behavior of capillary force have a complex dependency on many factors such as particle and pore size (Öberg and Sällfors 1997), water content or matric suction (Cho and Santamarina 2001), pore-air and pore-water pressures (Lu and Likos 2004), and the properties of the multiphase fluid interface (e.g., air–water surface tension, contact angle) (Lu and Khorshidi 2015; Lu and Zhang 2019).

When the soil mass dries further (high suctions), the capillary regime changes to an adsorption regime in which some of soil particles are not coated by thick water films anymore and liquid-filled corners are further connected through thin liquid films coating exposed solid surfaces (Kemper 1960; Dulien et al. 1986; Tuller et al. 1999; Or and Tuller 2002). The thin liquid film (called adsorptive water) is adsorbed on the soil surface through interfacial forces (called adsorptive forces) caused by electromagnetic fields of physicochemical forces known as van der Waals attraction, electrical double-layer repulsion, exchangeable cations, and surface hydroxyls forces (Lambe 1960; Sridharan and Rao 1973; Gens and Alonso 1992; Delage and Graham 1996; Romero and Simms 2008; Koliji et al. 2010; Lin and Cerato 2014). The adsorptive forces can play an important role in the structure and overall mechanisms behavior of fine-grained soils depending on soil specific area and clay content (the larger the relative surface area, the larger the interfacial adsorptive forces) (Banin and Amiel 1970; McQueen and Miller 1974; Karathanasis and Hajek 1982; Grismer 1987).

The development of tensile strength in a drying soil mass can be explained if both capillary and adsorptive bonding forces are known. While several models exist in the literature that can

predict the tensile strength for a specific range of water content (or suction) and soil type, there is dearth of studies in the literature that propose a comprehensive model for the prediction of the tensile strength of a variety of unsaturated soils ranging from clean sands to silty and clayey soils. In most cases, the capillary and adsorptive forces are lumped together without distinguishing individual contributions. This study presents a general model for the tensile strength characteristic curve (TSCC), which establishes a relationship between the tensile strength versus water content in unsaturated soils. The proposed model is applicable to various soil types ranging from clean sands to silty and clayey soils. Tensile strength is characterized using the suction stress concept and the TSCC model is built upon the concept that changes in tensile strength with water content (or degree of saturation) are separately controlled by two distinct water retention mechanisms of capillarity and adsorption. Predications from the proposed model and several alternative models were then compared against laboratory measured tensile strength reported in the literature for ten different soils.

### 3.2 Background

Some researchers developed tensile strength models using micro-mechanics approaches considering that capillary and adsorptive bonding forces take place at the micro scale, (Haines 1925; and Fisher 1926; Rumpf 1970). For example, assuming that soils are idealized as noncolloidal materials consisting of uniformly rigid spheres at regular packing states, Haines (1925) and Fisher (1926) correlated the cohesion induced by the interparticle capillary forces, which must be counterbalanced by applied tensile stress for tensile failure, to water content and particle radius. Rumpf (1970) investigated the variation of the tensile strength in both the pendular regime (residual regime) and the capillary regime on the assumption that the real soil particles are smooth particles with a finite surface separation. In the pendular regime, they statically related tensile strength between adjacent particles, porosity, and the mean size of particles, while in the capillary regime, they simply approximated the tensile strength of granular materials to the capillary pressure (Rumpf 1970). Following Rumpf's theory, Pietsch (1968) estimated the tensile strength of granular materials in the entire moisture range assuming that the tensile strength increases linearly with the degree of saturation from a critical point of saturation, where water bridges in the aggregates begin to connect to each other. Schubert (1975) calculated the tensile strength in the capillary regime by multiplying capillary pressure with degree of saturation. For the funicular regime, however, they derived tensile strength from a linear relationship between the bonding force (originating from water bridges and that caused by saturated pores filled with bulk water) and the degree of saturation. Although the micro-mechanics approach can fundamentally explain the mechanisms associated with the

development of the tensile strength, they are limited to use in practice due to the oversimplified assumptions.

Upscaling and lumping together the microscopic interparticle stresses arising from capillary and adsorptive forces, some studies have used the concept of effective stress as a macro-mechanics approach to develop correlations between tensile strength and degree of saturation (water content or soil suction) (e.g., Snyder and Miller 1985; Péron et al. 2009; Lu et al. 2009; Tang et al. 2015; Yin and Vanapalli 2018) when the effective stress of the soil at failure equals zero. For example, following Bishop's effective stress principle (Bishop 1959), which is a macroscale approach for describing the state of stress in unsaturated soils, Snyder and Miller (1985) proposed a tensile strength model for unsaturated soils. In another study, Péron et al. (2009) used Bishop's generalized effective stress principle to develop a tensile strength model. However, the applicability of these methods is limited in research and practice because of the difficulties associated with experimentally or theoretically determining Bishop's effective stress parameter (Yin and Vanapalli 2018). Lu et al. (2007; 2009) employed the suction stress concept (Lu and Likos 2006) for effective stress formulation to characterize the uniaxial tensile strength in unsaturated sands by employing the nonlinear Mohr-Coulomb failure criterion. Suction stress is a stress variable upscaling and summing all interparticle forces including physicochemical forces (i.e., van der Waals forces, electrical double-layer forces, chemical cementation forces at the grain contacts), and capillary forces (Lu and Likos 2006; Lu et al. 2010). For sandy soils, where capillary forces are the only suction stress component, a non-monotonic trend between suction stress and degree of saturation is reported (Lu and Likos 2006). A too-dry or too-wet condition will diminish

interface areas or will result in small capillary stresses. However, for clayey soils, suction stress is not zero at dry or fully saturated conditions due to the presence of interfacial adsorptive forces. Based on this observation for clays, Tang et al (2015) added a residual tensile strength to the Lu et al. (2009) model originally developed for sands so they could estimate the tensile strength of low plasticity clay. The added residual tensile stress corresponded to the fully saturated state.

In addition to the effective stress approach, the interparticle forces can be characterized by another macro-mechanics approach, the apparent cohesion concept (cohesion between particles stemming from suction), which is the intercept of the Mohr-Coulomb failure envelope with the shear-stress axis at a specific matric suction (Fredlund and Rahardjo 1993). Combining the Mohr-Coulomb shear strength parameters and the soil water characteristic curve (SWCC), the tensile strength of unsaturated soils have been predicted by several researchers (e.g., Morris et al. 1992; Vanapalli et al. 1996; Lakshmikantha et al. 2012; Varsei et al. 2016). For example, Morris et al. (1992) proposed a tensile strength model by multiplying the intercept of the M-C failure envelope modified for unsaturated soils by Fredlund et al. (1978) on the horizontal axis with an empirical reduction factor. Lakshmikantha et al. (2012) used the M-C failure envelope modified for unsaturated soils by Alonso et al. (2010) to derive an isotropic tensile strength model for a low silty clay. In a following study, Varsei et al. (2016) used the same failure model to propose a uniaxial tensile strength for two clays by solving Mohr's circle for zero major principal stress. Yin and Vanapalli (2018) reviewed these models and concluded that these models were valid for a medium range of saturation around optimum moisture content, not for the entire range of water contents.

Additionally, various empirical models between tensile strength and soil suction or water content (or degree of saturation) have been constructed from tensile strength experimental data using the regression analysis (e.g., Kim and Hwang 2003; Zeh and Witt 2005; Trabelsi et al. 2012). For example, Zeh and Witt (2005) proposed a model for a medium plasticity soil based on suction-controlled modified triaxial tests for a wide range of degree of saturation. In a review, Yin and Vanapalli (2018) compared this model with the linear empirical model proposed by Lutenegger and Rubin (2008). Although, the model proposed by Zeh and Witt (2005) represented the trend of the variation of tensile strength over a wide range of water contents, it neither well predicted the tensile strength for the very dry end (extremely high suction) nor it was applicable to the soils with different properties from medium plastic clays. The linear empirical model proposed by Lutenegger and Rubin (2008) covered more soils (four fine-grained soils), but it was only valid for the water content range around the optimum water content. In a following study, Trabelsi et al. (2012) proposed another empirical model for the prediction of the tensile strength of a highly plastic clay with respect to soil suction. Due to the validation of empirical models for a limited range of soils and water contents, these models could not be considered as generalized methods to predict the tensile strength and failure in earthen structures built in different types of soils and exposed to various ranges of water regimes Venkataramana et al. (2009).

In summary, although these theoretical and empirical models can predict the tensile strength for a specific range of water content (or suction) and soil type, they are not intended to predict the tensile strength of a variety of unsaturated soils ranging from clean sands to silty and clayey soils over a wide range of water content.

### 3.3 Tensile Strength Characteristic Curve Model

Fig. 3. 1a depicts a soil element within a soil mass subjected to a tensile stress applied normal to one principal plane, with zero stress applied to the corresponding orthogonal planes (uniaxial tensile stress). When the applied uniaxial tensile stress reaches the tensile strength, failure occurs, and tensile cracks develop (Fig. 3. 1b). In other words, the interparticle bonding forces are counterbalanced along the failure plane. This state of stress is shown in the $\tau - \sigma$ space as point A on the left side of the graph as normal stress is tensile with a negative sign (Fig. 3. 1c). In this study, the Mohr-Coulomb envelope is used to develop the TSCC model. The Mohr-Coulomb envelope describes observed relationships between normal stress (either effective or total) and shear stress at failure, as established by various forms of soil testing with the preponderance of tests being triaxial compression shearing. Further, it has been observed that the intercept of the Mohr-Coulomb envelope on the normal stress axis is, in fact, strongly related to observed tensile strengths from various types of tests (Lu et al. 2009; Tang et al. 2015; Yin and Vanapalli 2018). Therefore, the Mohr-Coulomb envelope is appropriate to use in a model that predicts tensile strength. The interparticle bonding forces act in all directions and correspond to the isotropic tensile strength meaning that there is no shear stress component in any direction (point B in the $\tau - \sigma$ space) (Fig. 3. 1c). It is noteworthy that point B is referred to as opening mode (mode I) in fracture mechanics for describing cracks when no shear/frictional stress is applied (Snyder and Miller 1985; Hueckel et al. 2014). From point B, the Mohr-Coulomb failure envelope can be extended if soil friction angle ($\phi$) is known assuming that shear strength is a linear function of normal stress. There is empirical evidence to suggest that the friction angle under tension or

compression is likely similar, and therefore in the current study, it is assumed that the ratio of shear strength to normal stress remains constant in both compressive and tensile regimes (tan $\phi$). Now, if the isotropic tensile strength (point B) is known, the uniaxial tensile strength (point A) can be determined by constructing a Mohr's circle through point A and tangent to the failure envelope.

In this study, we present a general TSCC model by exploring the Lu et al. (2009)'s hypothesis that changes in tensile strength with water content (or degree of saturation) are controlled by water retention mechanisms. In this paper however, two distinct water retention mechanisms of capillarity and adsorption are incorporated. In a pioneering study, Tuller et al. (1999) developed a soil water retention curve (SWRC) model separately considering capillary and adsorptive water regimes. They developed a scaling relationship between water content and specific surface area to estimate water retention in the dry end separately from capillary water retention. In a following work, Lu (2016) proposed a new SWRC model to distinguish adsorption and capillary mechanisms and incorporated additional features such as cavitation and the highest matric suction as follows:

$$\theta(\psi) = \theta_a(\psi) + \theta_c(\psi) \quad \textbf{(3- 1)}$$

$$\theta_a(\psi) = \theta_{amax}\left\{1 - \left[exp\left(\frac{\psi - \psi_{max}}{\psi}\right)\right]^m\right\} \quad \textbf{(3- 2)}$$

$$\theta_c(\psi) = \frac{1}{2}\left[1 - erf\left(\sqrt{2}\frac{\psi - \psi_c}{\psi_c}\right)\right][\theta_s - \theta_a(\psi)][1 + (\alpha\psi)^n]^{1/n-1} \quad \textbf{(3- 3)}$$

where $\theta_a(\psi)$ is adsorbed water; $\theta_c(\psi)$ is capillary water; $\psi$ is matric potential; $\theta_{amax}$ is adsorption capacity; $\psi_{max}$ is highest suction corresponding to zero water content; m is

adsorption strength; erf () is error function (Mathews and Walker 1970); $\psi_c$ is mean cavitation suction; $\theta_s$ is saturated volumetric water content; $\alpha$ is fitting parameter related to the air entry suction; *n* is fitting parameter related to pore-size distribution.

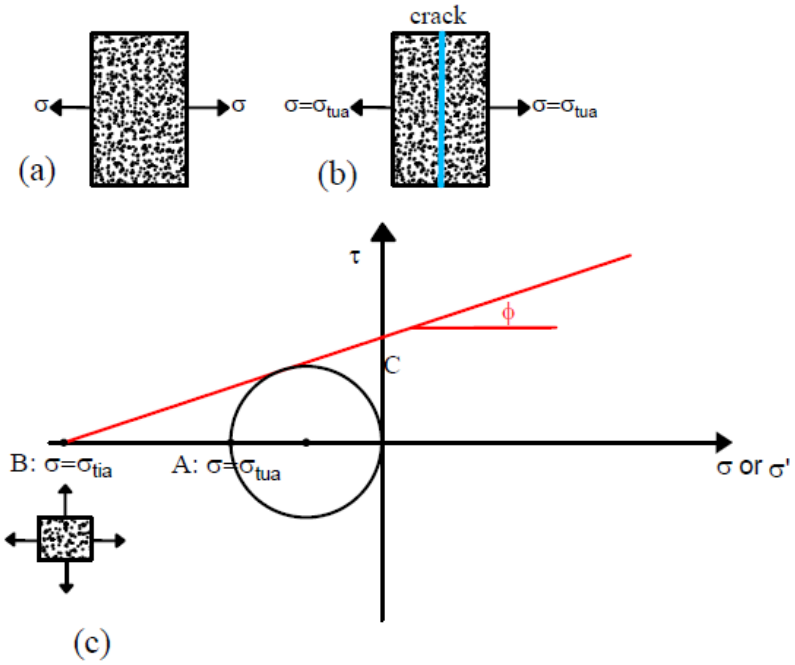



**Figure 3. 1. a. Uniaxial tensile strength; b. uniaxial tensile strength at failure; c. conceptual illustration of isotropic tensile strength $\sigma_{tia}$ and uniaxial tensile strength $\sigma_{tua}$ based on the concept of suction stress for Mohr-Coulomb criterion failure (modified after Lu et al., 2009).**

In these equations, $\theta_{amax}$, which is equivalent to the residual water content $\theta_r$, is used to distinguish the adsorptive water regime from the capillary water regime, meaning that adsorption is dominant below $\theta_r$ while capillarity is dominant above $\theta_r$. However, the transition water content from adsorptive water regime to capillary water regime is higher than the residual water content, $\theta_r$, especially in clays when there is a considerable amount of adsorptive water in addition to capillary water (Tuller and Or 2005). In sands, the residual water content can be an accurate representative of the transition point as the capillary regime is the dominant water component. For this reason, many studies have shown that a SWRC model does not properly account for the effect of adsorption or cannot accurately capture laboratory measured SWRC data in the adsorption stage for silts and clays (e.g., Lu and Likos 2004, 2006; Lu et al. 2010).

To define a unified effective stress for unsaturated soils ranging from sands to silts and clays, Zhang and Lu (2020) built a two-part suction stress characteristic curve (SSCC) model based on Lu (2016) SWRC model (Eq. 1-3) considering adsorptive and capillary effects as two separate mechanisms as follows:

$$\sigma_{ads}^{s}(w) = f_{ads}(w)\sigma_{dry}^{s} \quad \textbf{(3- 4)}$$

$$f_{ads}(w) = \frac{1}{2}\left[1 - \operatorname{erf}\left(\beta \frac{w - w_{tran}^{ss}}{w_{tran}^{ss}}\right)\right] \quad \textbf{(3- 5)}$$

$$\sigma_{cap}^{s}(w) = -\frac{f_{cap\,(w)}}{\alpha^{ss}}\frac{w}{w_s}\left[\left(\frac{w}{w_s}\right)^{n^{ss}/1-n^{ss}} - 1\right]^{1/n^{ss}} \quad \textbf{(3- 6)}$$

$$f_{cap}(w) = \frac{1}{2}\left[1 + \operatorname{erf}\left(4 \frac{w - w_{tran}^{ss}}{w_{tran}^{ss}}\right)\right] \quad \textbf{(3- 7)}$$

$$\sigma^S(w) = \sigma^S_{ads}(w) + \sigma^S_{cap}(w) \quad \textbf{(3- 8)}$$

where $\sigma^S_{ads}(w)$ is adsorptive suction stress; $f_{ads}(w)$ is a dimensionless scaling function reflecting the distribution of physicochemical forces in terms of probability; $\sigma^S_{dry}$ is suction stress at the oven-dry state; $\beta$ is dimensionless parameter reflecting the strength of adsorptive suction stress which determines the transition between adsorption and capillarity; $w^{ss}_{tran}$ represents the water content where adsorption water regime transitions to capillary water regime as shown in Fig. 3. 2 (the range of $w^{ss}_{tran}$ changes from 0 for clean sands to as high as 0.35 for expansive clays) (Zhang and Lu 2020); $w_s$ is saturated gravimetric water content; $\sigma^S_{cap}(w)$ is capillary suction stress; $\alpha^{ss}$ is a fitting parameter related to the inverse of the average capillary suction stress depending mainly on the average pore size, soil type and void ratio (the larger the pore sizes, the higher $\alpha^{ss}$ values); $n^{ss}$ is a fitting parameter related to the pore-size distribution for the capillary suction stress controlling the slope of the capillary suction stress between the transitional water and saturated water content (the range of $n^{ss}$ changes from 1.5 to 3) (Zhang and Lu 2020). Note that gravimetric water content was used in Eqs. (4-8) because the adsorptive component of the water content relates to the thickness of the thin film (the distance from the solid to the liquid-vapor interface) and only depends on soil mass not void ratio or porosity (Philip 1977; Zhang and Lu 2018). Therefore, in this study, gravimetric water content is used instead of volumetric water content.

At the oven-dry state when there is the least particle separation distance, the van der Waals force is at a maximum while the electrical double layer repulsion is small (Zhang and Lu 2020). Upon wetting, with an increase in particle separation distance, the van der Waals attraction force

weakens, and electrical double layer repulsion develops. Therefore, the maximum macroscale adsorptive suction stress, $\sigma_{dry}^{s}$, occurs at an oven-dry state and decreases with an increase in water content. Eq. (4) can well model this trend of adsorptive suction stress with the use of the dimensionless scaling function $f_{ads}(w)$ (Eq. 5). $f_{ads}(w)$ varies from its maximum value of unity at the oven-dry state to its minimum value of zero at a fully saturated state. Also, $f_{cap}(w)$ as another dimensionless scaling function for capillarity water, changes from zero at an oven-dry state to unity at a fully saturated state.

In this study, the two-part SSCC model proposed by (Zhang and Lu 2020) is incorporated into the development of the TSCC model to separately account and distinguish interparticle forces and the resultant tensile strength under capillary and adsorptive mechanisms. Isotropic tensile strength (the microscopic interparticle stresses) arises from capillary and adsorptive forces, which are defined and upscaled by a stress variable called suction stress (Lu et al. 2009). So, suction stress (isotropic tensile strength) acts in all directions and there is no shear stress component in any direction meaning that no shear/frictional stress is applied (as it is the case in cracking). We take the sum of adsorptive and capillary suction stresses (Eq. 4 and Eq. 6) as an isotropic tensile stress (point B). Now, the uniaxial tensile strength (point A) can be determined by constructing a Mohr's circle through point A and tangent to the failure envelope as follows:

$$\sigma_{tu}(w) = 2\sigma_{tia}(w)\, tan\, \phi\, tan\left(\frac{\pi}{2} - \frac{\phi}{4}\right) \quad \textbf{(3- 9)}$$

$$\sigma_{tia}(w) = \sigma^{s}(w) = \sigma_{ads}^{s}(w) + \sigma_{cap}^{s}(w) \quad \textbf{(3- 10)}$$

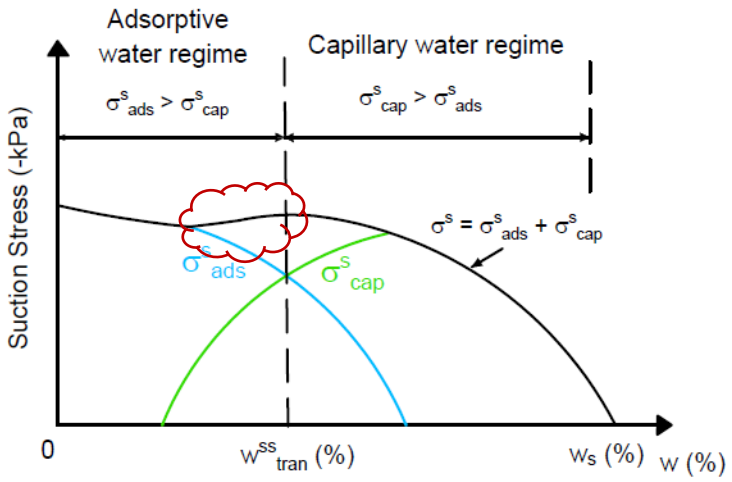



**Figure 3. 2. Conceptual illustration of suction stress curve incorporating both capillarity and adsorption (modified after Zhang and Lu, 2020).**

### 3.4 Validation and Comparison

The proposed TSCC model was validated against laboratory-measured tensile strength reported in the literature for ten different soils ranging from sand, silt, and clay. In these tests, the soil specimens were compacted at the same density but different initial target water contents, representing tensile strength of different soils at the same specific density and various initial water contents. Conventional direct tensile testing is carried out at constant water content or under constant suction conditions. In this case, the tensile strength is measured by externally applying tensile boundary forces that create internal tensile stresses in the soil (e.g., Frydman 1964; Bishop and Garga 1969; Ajaz and Parry 1975; Tang and Graham 2000; Nahlawi et al. 2004; Tamrakar et al. 2005; Vesga 2009; Lakshmikantha et al. 2012; Tang et al. 2015). Fig. 3. 3 shows

the hypothetical stress path (AB) for this case when tensile strength is determined at a constant water content. In another attempt, Varsei et al. (2016) designed a desiccation test apparatus to measure the tensile strength directly during desiccation process. In this case, the tests are decreasing water content tests (increasing suction) where internally developed tensile stresses produce measurable external boundary forces. Path CB shown in Fig. 3. 3 corresponds to the hypothetical stress path for the desiccation case when water content changes.

Further, the predictive accuracy of the proposed model is compared against four alternative models proposed by Lu et al. (2009), Tang et al. (2015), Varsei et al. (2016), and Yin and Vanapalli (2018). Table 3. 1 shows basic geotechnical parameters of the soils used for validation and comparison purposes. Table 3. 2 presents the TSCC model parameters for these ten soils. To statistically examine the predictive accuracy of the models, the coefficient of determination, $R^2$, and the root mean square error (RMSE) were determined for each model and soil. The RMSE is a statistical measure used to quantify the variation (error) between each tensile strength from each predictive model and laboratory-measured data obtained from the literature. High accuracy is indicated by a RMSE that is close to zero, and a $R^2$ that is close to unity. As defined, $\sigma_{dry}^{s}$ equals the suction stress at the dry end of the curve which can be measured in the lab. In this study, in the absence of laboratory-measured $\sigma_{dry}^{s}$, we used the following equation proposed by Tuller and Or (2005) between water content and specific surface area at the dry end to determine $\sigma_{dry}^{s}$:

$$w = \sqrt[3]{\frac{A_{svl}}{6\pi\rho_w g\Pi}} SA\rho_w \qquad \textbf{(3- 11)}$$

where $w$ is gravimetric water content; $A_{svl}$ is the Hamaker constant value of -6 × $10^{-20}$ J; $\rho_w$ is the density of water in kg/$m^3$; $g$ is the acceleration of gravity in m/$s^2$; *SA* is specific surface area in $m^2$/kg; $\Pi$ is the interfacial force per unit area. This relationship was developed based on a simple assumption that a liquid film is absorbed on a planer surface due to interfacial interactions induced by van der Waals forces only (Tuller et al. 1999). In the current study, $\Pi$ is considered as $\sigma_{dry}^{s}$ at the dry end of the curve. Note that Eq. (11) is developed for specific surface areas smaller than 200 $m^2$/kg. To make sure about the applicability of this equation in the estimation of $\sigma_{dry}^{s}$, the results from Eq. (11) were compared to the experimental measurements for $\sigma_{dry}^{s}$ presented by Zhang and Lu (2020). A good agreement between the measured and calculated $\sigma_{dry}^{s}$ using Eq. (11) was observed, leading us to use Eq. (11) for the estimation of $\sigma_{dry}^{s}$ in this study in the absence of laboratory-measured $\sigma_{dry}^{s}$. The remaining SSCC parameters were deduced based on the suggestions made by Zhang and Lu (2020). For example, $\beta$ was suggested to be 4.0 for low-expansive and non-expansive soils and 2.0 for expansive and high-expansive soils (Zhang and Lu 2020).

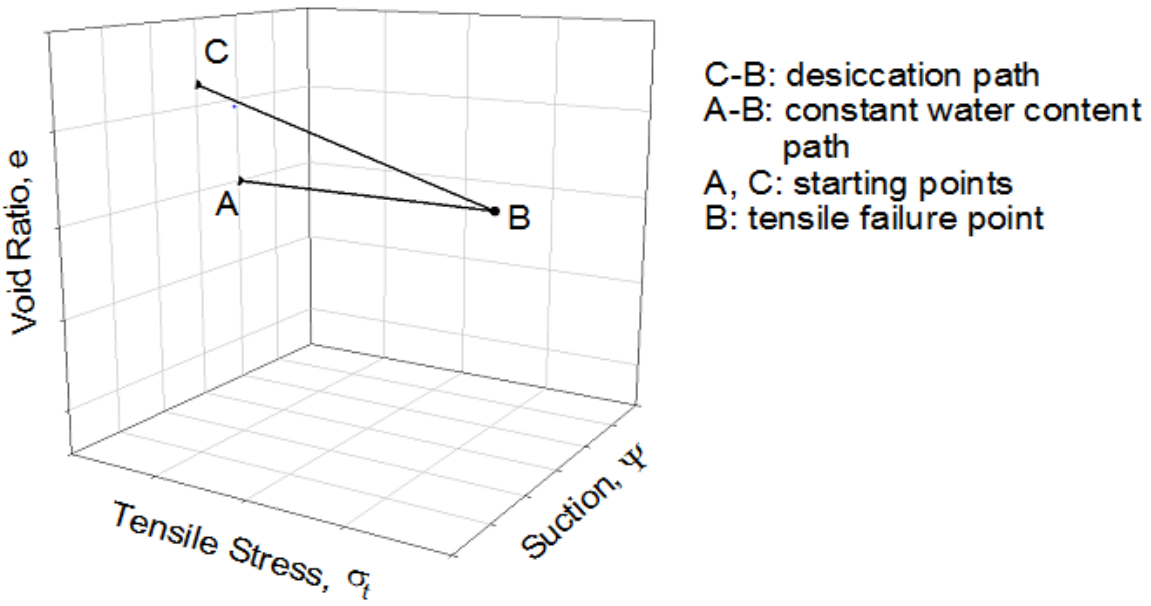



**Figure 3. 3. Hypothetical stress paths for a desiccation test and for a constant water content tensile strength test**

**Table 3. 1. Basic geotechnical parameters of soils used for model validation and comparison.**

| Soil | USCS | LL (%) | PL (%) | PI | Specific gravity | $\emptyset'$ (deg.) | Source |
|---|---|---|---|---|---|---|---|
| Esperance sand | SP | _ | _ | _ | 2.80 | 50.0 | Lu et al. (2009) |
| Perth sand | SP | _ | _ | _ | 2.65 | 48.0 | Lu et al. (2007) |
| Silica sand | SP | _ | _ | _ | 2.65 | 56.0 | Jindal et al. (2016) |
| Manchester silt | ML | _ | _ | _ | 2.70 | 35.0 | Snyder (1980) |
| Laronde mine tailing silt | ML | _ | _ | _ | 2.75 | 30.0 | Narvaez et al. (2015) |
| Idabel clay | CH | 72 | 26 | 46 | 2.78 | 15.6 | Salimi et al. (2021) |
| Chickasha clay | CL | 38 | 20 | 18 | 2.57 | 29.0 | Salimi et al. (2021) |
| Nanjing clay | CL | 37 | 20 | 17 | 2.73 | 29.0 | Tang et al. (2015) |
| Plessa clay | CL | 44 | 21 | 23 | 2.65 | 25.0 | Zeh and Witt (2005) |
| Glacial Till | CL | 45 | 24 | 21 | 2.65 | 25.0 | Stirling et al. (2015) |

**Table 3. 2. Parameters of the proposed TSCC model for different soils.**

| Soil | Void ratio | $\alpha^{SWR}$ (kPa$^{-1}$) | $n^{SWR}$ | $\sigma^{s}_{dry}$ (-kPa) | $\alpha^{ss}$ (kPa$^{-1}$) | $n^{ss}$ | $w^{ss}_{tran}$ (g/g) | $\beta$ | $w_s$ (g/g) |
|---|---|---|---|---|---|---|---|---|---|
| Esperance sand | 0.82 | 0.700 | 4.0 | 0 | 0.700 | 3.8 | 0.01 | 4 | 0.28 |
| Perth sand | 0.67 | 0.700 | 4.0 | 0 | 0.700 | 4.0 | 0.01 | 4 | 0.25 |
| Silica sand | 0.65 | 0.500 | 3.0 | 0 | 0.500 | 2.9 | 0.01 | 4 | 0.25 |
| Manchester silt | 0.73 | 0.015 | 4.0 | 1 | 0.017 | 4.0 | 0.01 | 4 | 0.27 |
| Laronde mine tailing silt | 0.84 | 0.006 | 1.9 | 40 | 0.006 | 1.9 | 0.01 | 4 | 0.31 |
| Idabel clay | 1.07 | 0.012 | 1.5 | 160 | 0.008 | 2.0 | 0.19 | 2 | 0.39 |
| Chickasha clay | 0.66 | 0.026 | 1.5 | 80 | 0.020 | 2.0 | 0.13 | 2 | 0.26 |
| Nanjing clay | 0.71 | 0.008 | 1.9 | 100 | 0.008 | 1.8 | 0.10 | 2 | 0.26 |
| Plessa clay | 0.37 | 0.002 | 1.6 | 700 | 0.002 | 1.7 | 0.05 | 2 | 0.14 |
| Glacial Till | 0.61 | 0.005 | 1.6 | 400 | 0.005 | 1.7 | 0.08 | 2 | 0.23 |

To better understand the concept of adsorptive and capillary water in unsaturated soils, we first analyze the SWRC and SSCC for the ten different soils. Figs. 3. (4 and 5) show the generalized SWRC proposed by Lu (2016) for sand/silts and clays, respectively. For three sands and two silts shown in Fig. 3.  4, the SWRCs are quantified mainly by the capillary water and there is not a noticeable transition from the capillary regime to adsorbed film regime. However, a noticeable transition between these regimes is observed for the five clays as shown in Fig. 3.  5. For example, for the suctions higher than 6500 kPa in Idabel clay, the adsorption is the dominant water retention mechanism and changes in water content mainly reflect changes in adsorption water. SSCCs for the mentioned soils are presented in Figs. 3. (5 and 6). Again, capillary bonding forces are responsible for the development of total suction stress for sands and silts (Fig. 3. 5), suction stress vanishes at both the dry and wet sides. While adsorptive bonding forces have shown to have a significant impact on the development of suction stress in clays (Fig. 3. 6) and a comparable amount of adsorptive suction stress is developed in clays leading to an increasing trend in suction stress in the dry side. As mentioned before, this behavior in clays is due to their high specific surface area.

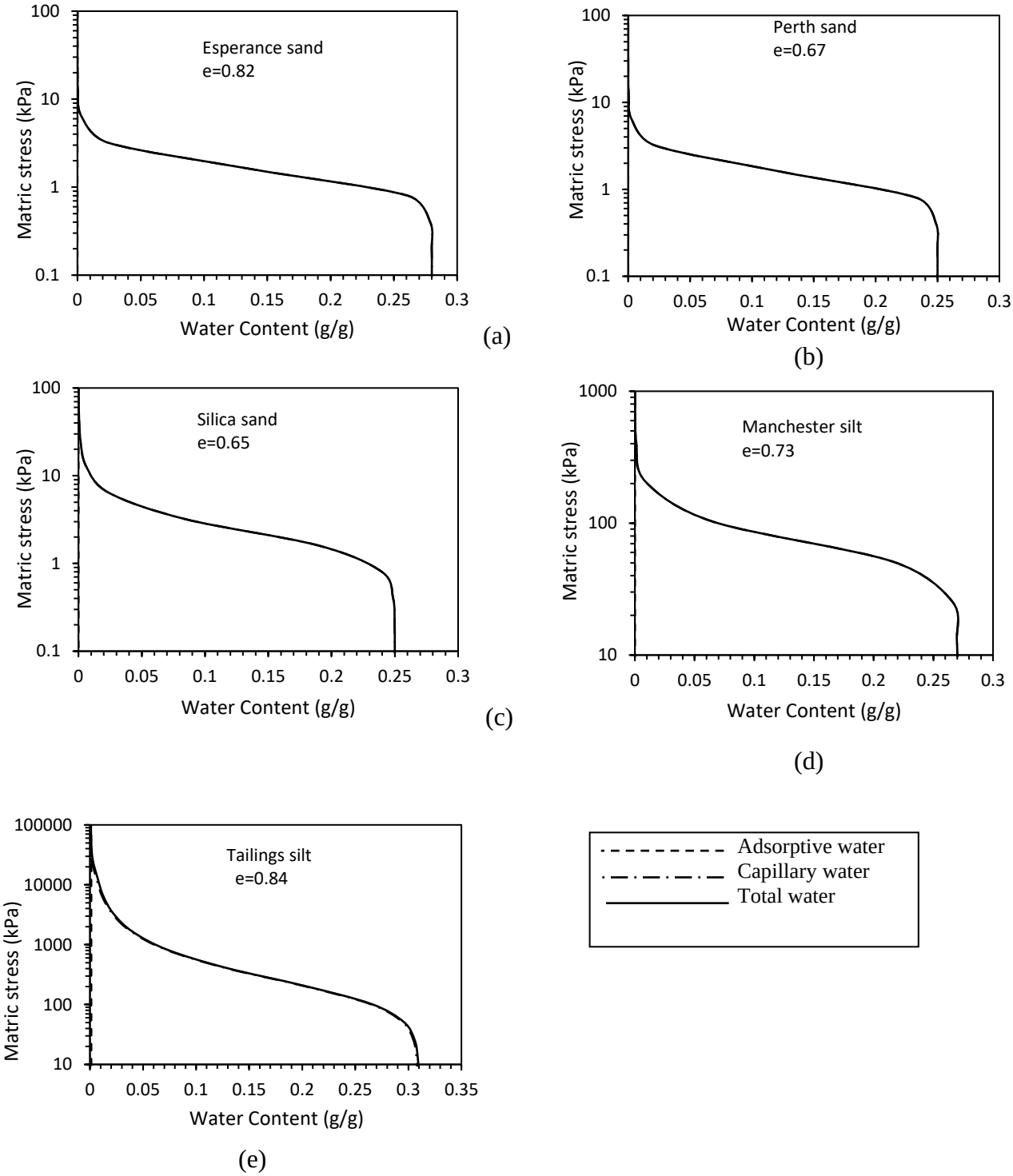



**Figure 3. 4. SWRC: (a) Esperance sand e=0.82; (b) Perth sand e=0.67; (c) Silica sand e=0.65; (d) Manchester silt e=0.73; (e) Tailings silt e=0.84.**

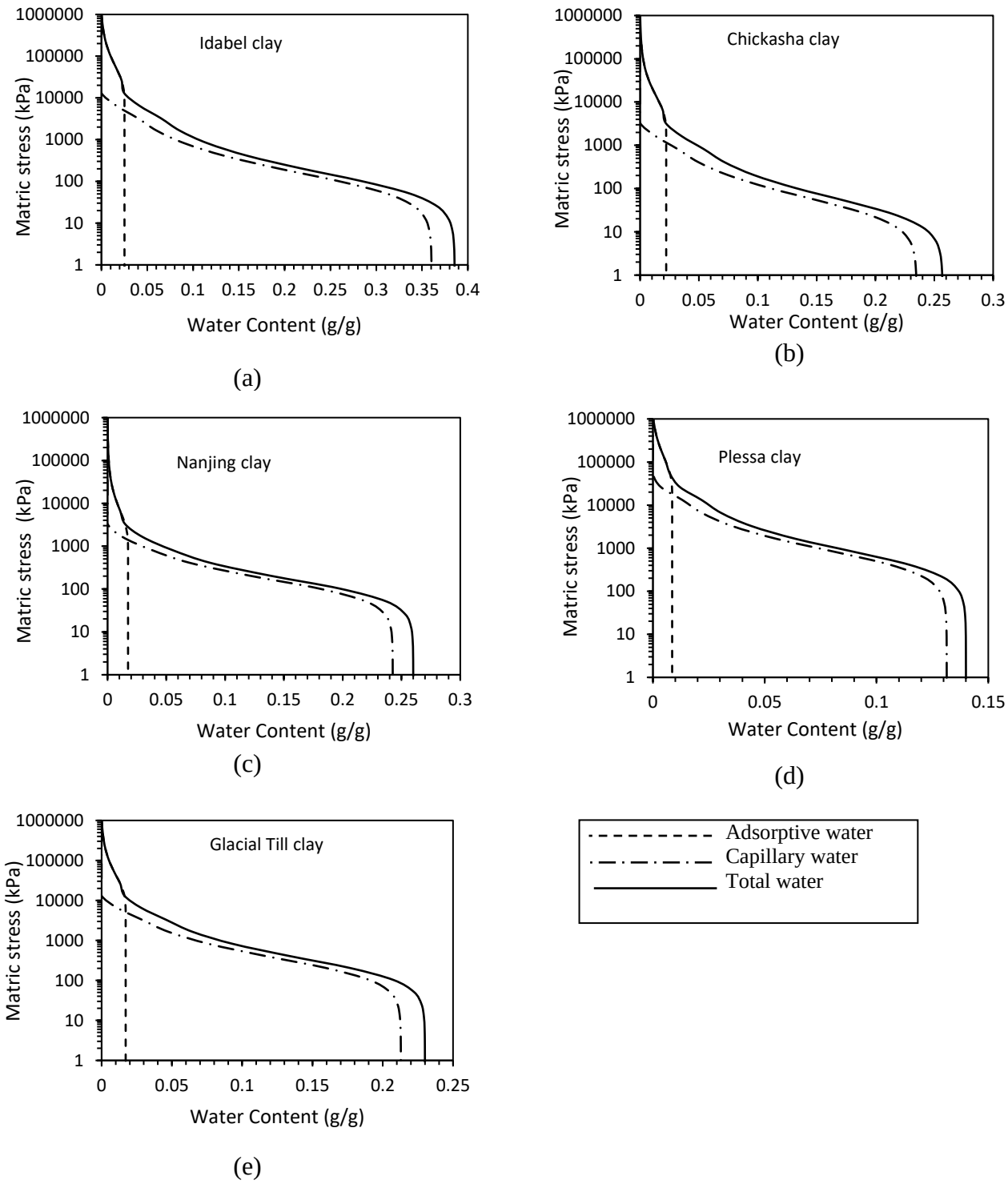



**Figure 3. 5. SWRC: (a) Idabel clay; (b) Chickasha clay; (c) Nanjing Clay; (d) Plessa clay; (e) Glacial Till clay.**

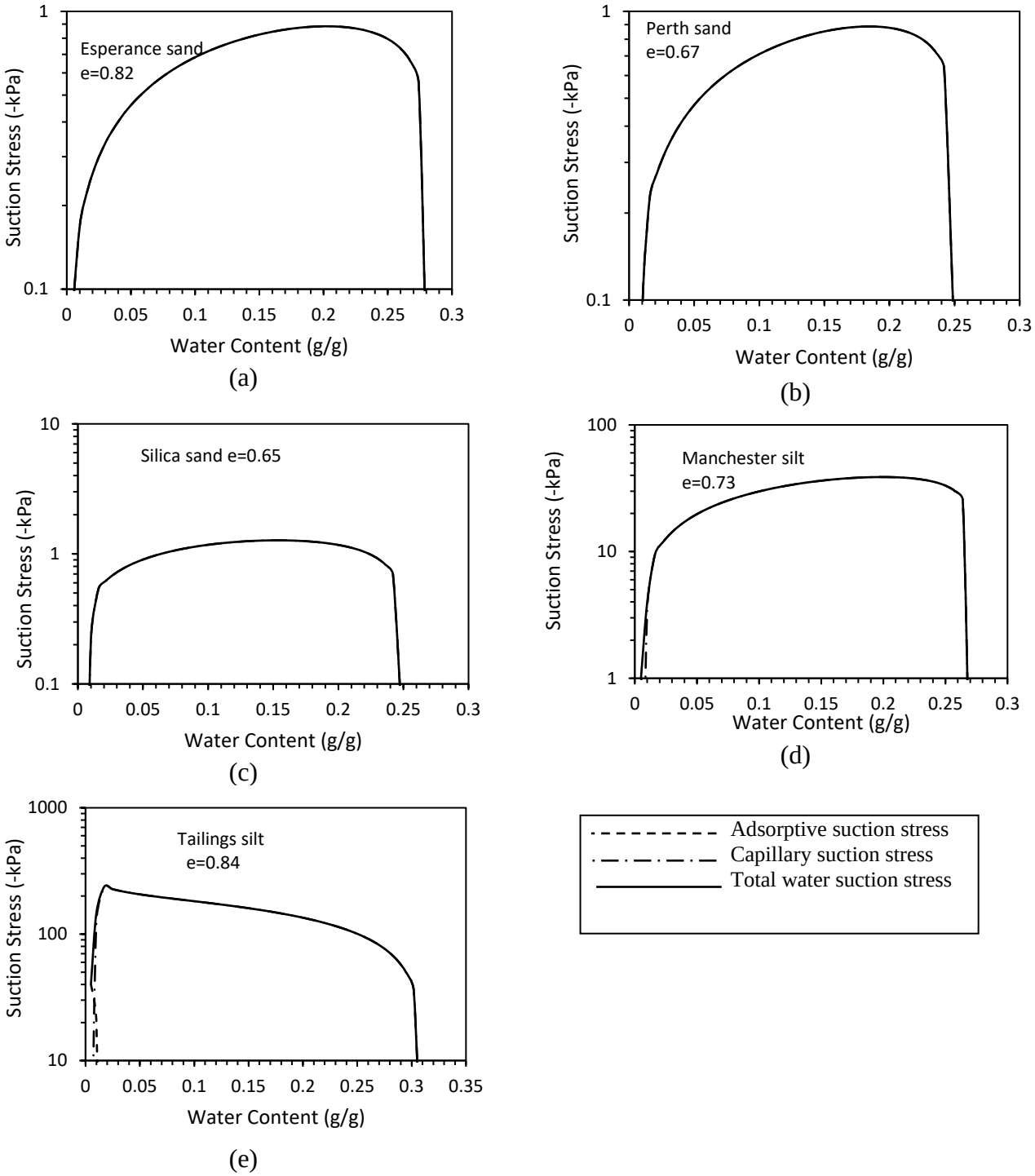



**Figure 3. 6. SSCC: (a) Esperance sand e=0.82; (b) Perth sand e=0.67; (c) Silica sand e=0.65; (d) Manchester silt e=0.73; (e) Tailings silt e=0.84.**

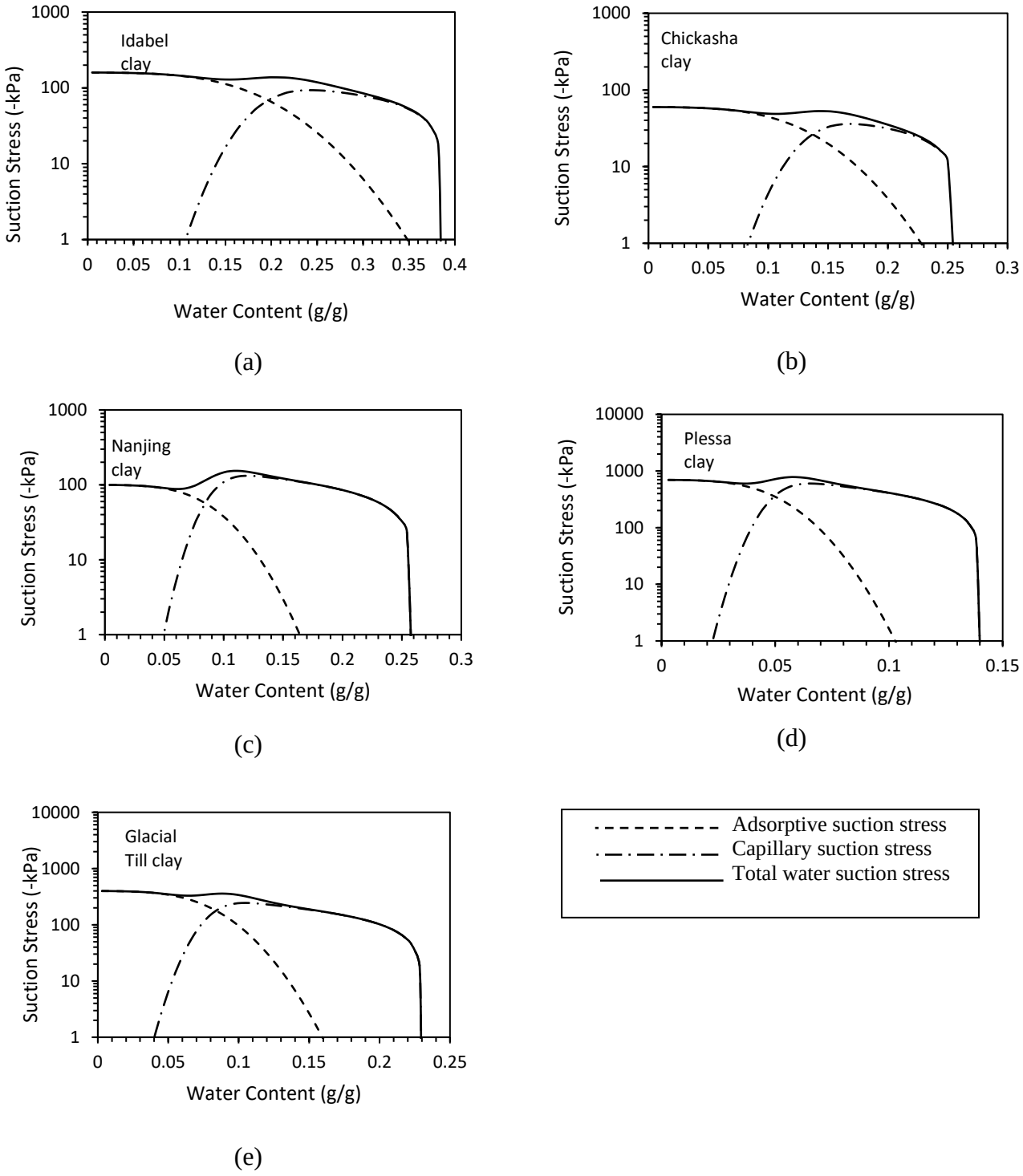



**Figure 3. 7. SSCC: (a) Idabel clay; (b) Chickasha clay; (c) Nanjing Clay; (d) Plessa clay; (e) Glacial Till clay.**

The uniaxial testing data along with the tensile strength predictions from the proposed model and Lu et al. (2009), Tang et al. (2015), Varsei et al. (2016), and Yin and Vanapalli (2018) models are shown for each soil in Fig. 3. 8(a-e). The $R^2$ close to unity and small RMSE values indicate that the models well represent the development of tensile strength in unsaturated sands (Figs. 3. 8(a-c) and Table 3. 3). The capillary interparticle force is the source of tensile strength in unsaturated sands and no adsorptive suction stress develops. The models are capable of predicting tensile strength due to capillary bonding force. As shown in Figs. 3. 8(d-e), a higher tensile strength was recorded for Manchester silt and Tailing silt. The capillary suction stress still is the dominant suction stress controlling the development of tensile strength in silts, although a small amount of adsorptive suction stress develops at the very dry side for Tailing silt shown in Fig. 3. 8(e).

The capability of different models to accurately predicit the tensile strength can be well distinguished when it comes to fine-grained soils (clays) where there is a noticeable amount of adsorptive water. As mentioned earlier, the existence of the adsorptive water regime and physicochemical forces affect the structure of clays. This means that in contrast to sands and most silts, the structure of clays does not remain constant over a wide range of water contents and changes from a floculated structure to a dispersed structure as the water content increases. The structure of clays can then affect the development of capillary interparticle bonding forces where both the adsorptive water and the capillary water exist ($\sigma^s_{ads}(w) \neq 0 \; and \; \sigma^s_{cap}(w) \neq 0$), red zone shown in Fig. 3. 2. In this zone, there are enough inter-aggregate pores in a soil specimen, and the capillary water is trapped between aggregates. As a result, water-bridges are formed in the contact points and the capillary bonding force develops leading to a higher tensile

strength even though the soil suction decreases (Salimi et al. 2021). When adsorptive water reduces to zero (when the red zone ends), the structure of clay turns into more of an aggregate-dispersed structure and water-bridges become gradually disconnected, resulting in a reduction in the capillary-induced tensile strength.

A TSCC model can well represent the development of tensile strength in clays if it takes into consideration the influence of the soil structure on the development of capillary interparticle forces. As presented in Table 3. 3, for Glacial Till clay, $R^2$ reduces from 0.75 for the general model proposed in this study to 0.48, 0.4, 0.16 and 0.32 for the models by Lu et al. (2009), Tang et al. (2015), Varsei et al. (2016), and Yin and Vanapalli (2018), respectively. The Lu et al. (2009) and Yin and Vanapalli (2018) models use residual water content $w_r$ to distinguish the adsorptive water regime from the capillary water regime, which is smaller than the real transition water content. As a result, they underestimate the influence of the adsorptive regime on the soil structure and the resultant tensile strength. Therefore, an increase in the tensile strength is observed as water content decreases or matric suction increases (Figs. 3. 9(a-e)). Tang et al (2015) model can describe the peak behavior by adding a residual tensile strength to the Lu et al. (2009) model, but only for a limited range of water contents around the optimum water content. Adding a residual tensile strength does not change the trend of the graphs for the very dry end, Figs. 3. 9(a-e). The Varsei et al. (2016) model was constructed based on the Alonso et al. (2010) effective stress framework considering compacted soils as double-pore structures for the entire range of water contents. This assumption underestimates the influence of adsorptive water regime. The proposed tensile strength model can well represent the tensile strength trend in different clays

as it correctly defines location of the transitional water content, Figs. 3. 9(a-e). The lower RMSE values obtained for the proposed model supports the applicability of this model compared to the other tensile strength models (see Table 3. 3).

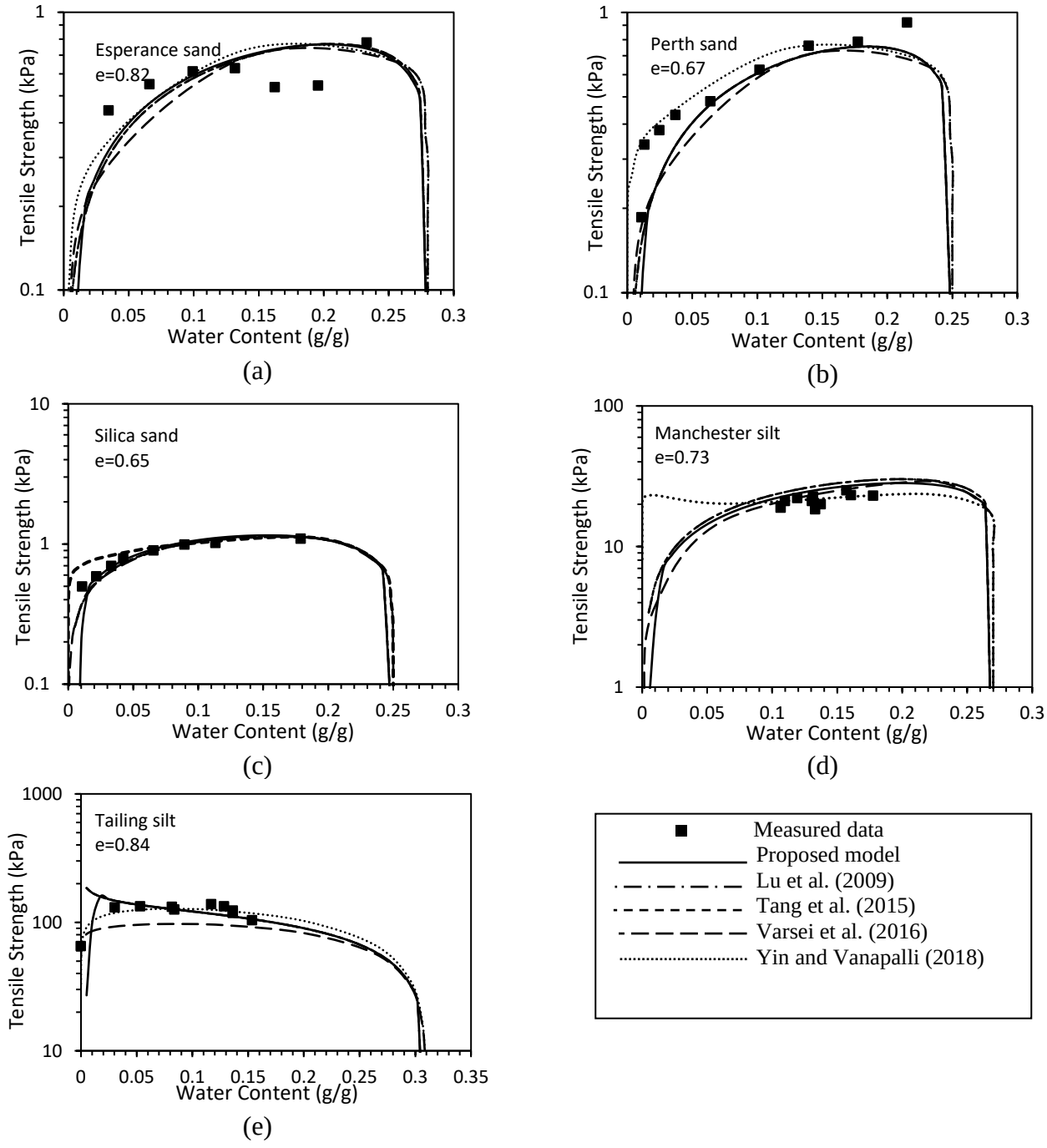



**Figure 3. 8. The comparison between tensile strength data with the tensile strength model predictions proposed by this study, Lu et al., (2009), Tang et al. (2015), Varsei et al. (2016), and Yin and Vanapalli (2018) for (a) Esperance sand e=0.82; (b) Perth sand e=0.67; (c) Silica sand e=0.65; (d) Manchester silt e=0.73; (e) Tailings silt e=0.84.**

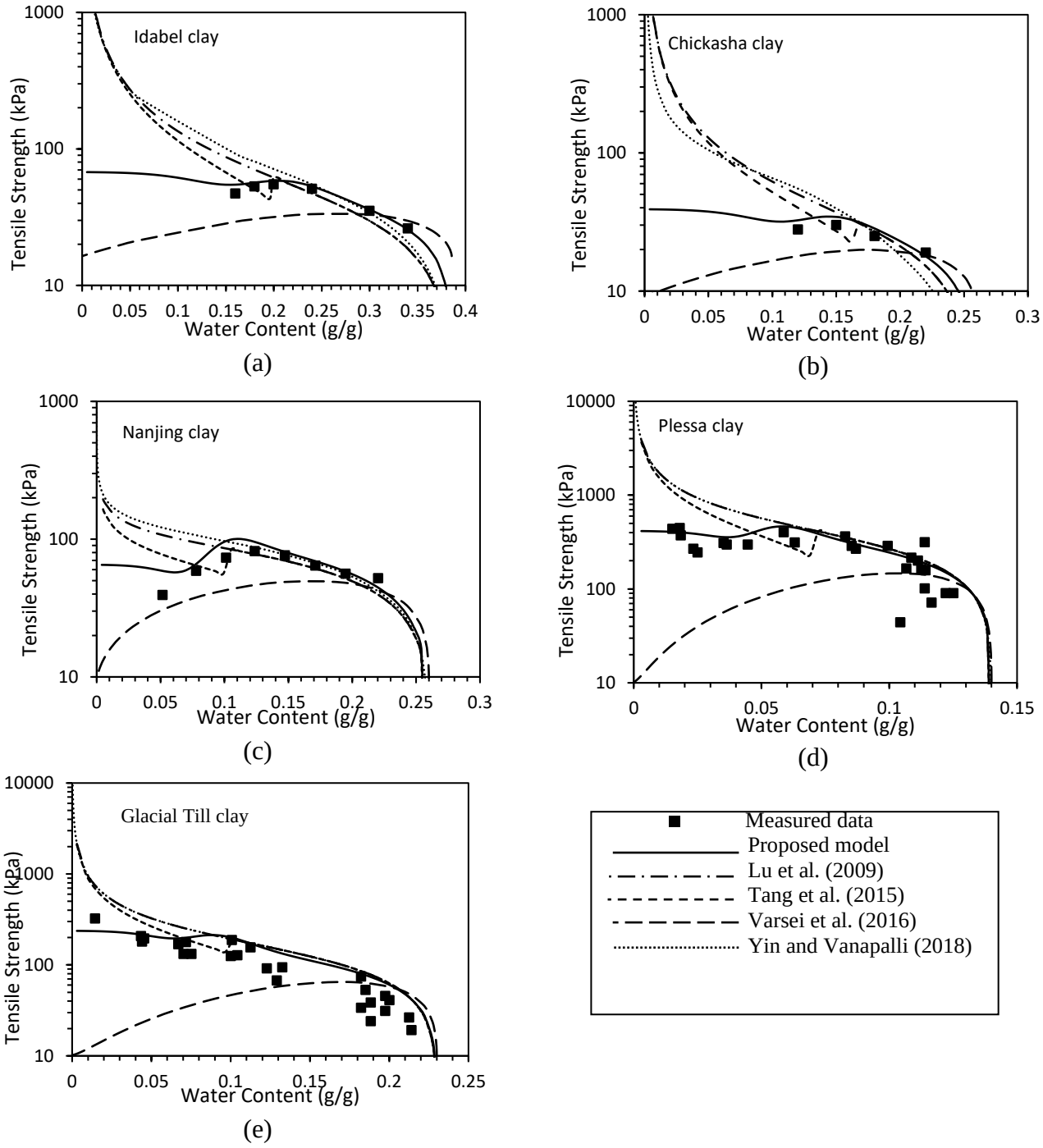



**Figure 3. 9. The comparison between tensile strength data with the tensile strength model predictions proposed by this study, Lu et al., (2009), Tang et al. (2015), Varsei et al. (2016), and Yin and Vanapalli (2018) for (a) Idabel clay; (b) Chickasha clay; (c) Nanjing Clay; (d) Plessa clay; (e) Glacial Till clay.**

**Table 3. 3. The coefficient of determination, R2, and the root mean square error (RMSE) of the proposed model and four alternative models in the perdition of laboratory measured tensile strength for different soils**

| Soils | | Proposed model | Lu et al. (2009) | Tang et al. (2015) | Varsei et al. (2016) | Yin and Vanapalli (2018) |
|---|---|---|---|---|---|---|
| Esperance sand (e=0.82) | RMSE | 0.10 | 0.10 | 0.10 | 0.11 | 0.09 |
| | $R^2$ | 0.78 | 0.75 | 0.75 | 0.72 | 0.81 |
| Perth sand (e=0.67) | RMSE | 0.07 | 0.07 | 0.07 | 0.06 | 0.03 |
| | $R^2$ | 0.85 | 0.89 | 0.89 | 0.79 | 0.97 |
| Silica sand (e=0.65) | RMSE | 0.05 | 0.03 | 0.03 | 0.04 | 0.08 |
| | $R^2$ | 0.90 | 0.97 | 0.97 | 0.95 | 0.80 |
| Manchester silit (e=0.73) | RMSE | 0.95 | 1.20 | 1.20 | 0.80 | 0.22 |
| | $R^2$ | 0.77 | 0.70 | 0.70 | 0.82 | 0.90 |
| Tailing silt | RMSE | 2.01 | 4.85 | 4.85 | 6.35 | 1.00 |
| | $R^2$ | 0.85 | 0.76 | 0.76 | 0.66 | 0.92 |
| Idabel clay | RMSE | 2.97 | 12.44 | 6.66 | 14.54 | 16.50 |
| | $R^2$ | 0.97 | 0.66 | 0.83 | 0.04 | 0.68 |
| Chickasha clay | RMSE | 3.38 | 10.32 | 5.63 | 6.64 | 11.28 |
| | $R^2$ | 0.99 | 0.69 | 0.56 | 0.10 | 0.71 |
| Nanjing clay | RMSE | 10.22 | 18.26 | 11.13 | 20.11 | 22.32 |
| | $R^2$ | 0.72 | 0.01 | 0.04 | 0.36 | 0.01 |
| Plessa clay | RMSE | 64.82 | 216.15 | 139.31 | 250.00 | 260.00 |
| | $R^2$ | 0.71 | 0.45 | 0.38 | 0.12 | 0.30 |

| | | | | | | |
|---|---|---|---|---|---|---|
| Glacial Till clay | RMSE | 56.32 | 195.46 | 140.01 | 221.04 | 251.32 |
| | $R^2$ | 0.75 | 0.48 | 0.40 | 0.16 | 0.32 |

# CHAPTER 4: A TEMPERATURE-DEPENDENT MODEL FOR TENSILE STRENGTH CHARACTERISTIC CURVE OF UNSATURATED SOILS

This chapter has been published as an article in the journal of Geomechanics for Energy and the Environment (Salimi, K., Cerato, A. B., Vahedifard, F., & Miller, G. A. (2021). A temperature-dependent model for tensile strength characteristic curve of unsaturated soils. Geomechanics for Energy and the Environment, 100244. https://doi.org/10.1016/j.gete.2021.100244). The paper has been reformatted and replicated herein with minor modifications in order to outfit the purposes of this dissertation.

## 4.1 Introduction and Background

The need for investigating the effect of elevated temperatures on the tensile strength is critical because: (1) the tensile strength plays the most important role in the formation and propagation of cracks in unsaturated soils (e.g., Tang et al. 2010; Kodikara and Costa 2013; Li et al. 2019; Zhu et al. 2020) and many of the processes leading to the formation of cracks in unsaturated soils involve elevated temperatures above the natural temperature variations (e.g., desiccation drying and wetting cycles) (McCartney et al. 2019); and (2) several applications, in which the formation of cracks can be detrimental and may lead to catastrophic failures, subject unsaturated soils to elevated temperatures. For examples, the influence of climate change and prolonged droughts on earthen structures (e.g., Vahedifard et al. 2015, 2016, 2018a); nuclear waste disposal (e.g., Ma and Hueckel 1992; Zheng et al. 2015); the high temperature caused by high voltage cables buried in the ground (e.g., Garrido et al. 2003; Salata et al. 2015); and energy geo-structures (e.g., Coccia et al. 2013; Stewart et al. 2014; Moradi et al. 2015; Başer et al. 2018).

There are different models for the determination of tensile strength of soils in the literature. For example, empirical models were constructed through regression analysis on the tensile strength experimental data (e.g., Kim and Hwang 2003; Zeh and Witt 2005; Trabelsi et al. 2012). Tensile strength can be analytically predicted if the interparticle bonding forces are known and reduce to zero along the failure plane (Ingles 1962; Santamarina 2003). There are some micro-mechanics analytical models which fundamentally explain the mechanisms associated with interparticle bonding forces and the resultant the tensile strength (Haines 1925; and Fisher 1926; Rumpf 1970). Moreover, there are some macro-mechanics analytical models to describe the tensile strength using the intercept of the Mohr-Coulomb failure envelope with the shear-stress axis at a specific matric suction (apparent cohesion) (e.g., Morris et al. 1992; Lakshmikantha et al. 2012; Varsei et al. 2016). In another macro-mechanics approach, tensile strength is described when the effective stress of the soil at failure equals zero (e.g., Lu et al. 2009; Tang et al. 2015; Yin and Vanapalli 2018). For example, Lu et al. (2009) showed that the combination of the Mohr-Coulomb failure criterion and the suction stress concept (Lu and Likos 2006) can precisely describe the uniaxial tensile strength in unsaturated sands. Suction stress is a stress variable representing all interparticle forces including physicochemical forces (i.e., van der Waals forces, electrical double-layer forces, chemical cementation forces at the grain contacts), and capillary forces.

The aforementioned empirical and micro/macro analytical models are predicting the tensile strength at ambient temperature and none of them can capture the effect of temperature on tensile strength. With that, the main objective of this study was to develop a temperature-

dependent model for the uniaxial tensile strength characteristic curve (TSCC) of unsaturated soils. The model is developed by employing the suction stress characteristic curve (SSCC) and extends upon the TSCC model recently developed by Salimi et al. (2021a) for ambient temperature to non-isothermal conditions by incorporating the effects of temperature into adsorptive and capillary suction stress components. The accuracy of the proposed TSCC model is validated with laboratory measured tensile strength data for two clayey soils tested at different temperatures ranging from 20 to 60 °C.

### 4.2 Tensile Strength Characteristic Curve

To properly model the temperature dependency of the TSCC, it is prudent to first identify key factors contributing to the development of tensile strength in unsaturated soils. A temperature dependent TSCC model can then be developed by quantifying the effects of temperature on those contributing factors. Salimi et al. (2021b) presented a model for determining the TSCC at ambient temperature. This study extends the TSCC model proposed by Salimi et al. (2021b) to temperature-dependent conditions. For completeness, the underlying theory, and key features of the Salimi et al. (2021b) model are recapitulated here. Interested readers are referred to Salimi et al. (2021b) for further details about the base model.

Tensile strength develops when the interparticle capillary and adsorptive forces reduce to zero. These interparticle forces are acting in all directions and correspond to the isotropic tensile strength meaning that there is no shear stress component in any direction. The capillary and adsorptive interparticle forces can be lumped into a single isotropic stress variable termed suction stress (Lu and Likos 2006; Lu et al. 2009). The intercept of the Mohr-Coulomb envelope on the normal stress axis has been proved to be strongly related to the isotropic tensile strength (suction stress) (Lu et al. 2009; Tang et al. 2015; Yin and Vanapalli 2018). Lu et al. (2009) and Salimi et al. (2021a) extended the Mohr-Coulomb failure envelope from the intercept on the normal stress axis by making two assumptions: 1) shear strength is a linear function of normal stress and 2) the ratio of shear strength to normal stress remains constant in both compressive and tensile regimes (tan $\phi$). Therefore, when suction stress and friction angle ($\phi$) are known, the uniaxial tensile strength can be determined by solving the Mohr's circle passing through the

origin. Suction stress, however, is shown to be temperature-dependent specifically in fine-grained soils (Vahedifard et al. 2019). Therefore, one can develop a temperature-dependent TSCC model by employing the temperature-dependent SSCC. Zhang and Lu (2020) proposed a new SSCC model separately considering adsorptive and capillary suction stresses. Using the Zhang and Lu (2020) SSCC model and Mohr-Coulomb's failure envelope, the following uniaxial TSCC model at ambient temperature is defined (Salimi et al. 2021a):

$$\sigma_{tu}(w) = 2\sigma_{tia}(w)\tan\phi\tan\left(\frac{\pi}{2}-\frac{\phi}{4}\right) \quad \textbf{(4- 1)}$$

$$\sigma_{tia}(w) = \sigma^{s}_{ads}(w) + \sigma^{s}_{cap}(w) \quad \textbf{(4- 2)}$$

$$\sigma^{s}_{ads}(w) = f_{ads}(w)\sigma^{s}_{dry} \quad \textbf{(4- 3)}$$

$$f_{ads}(w) = \frac{1}{2}\left[1 - \operatorname{erf}\left(\beta'\frac{w - w^{ss}_{tran}}{w^{ss}_{tran}}\right)\right] \quad \textbf{(4- 4)}$$

$$\sigma^{s}_{cap}(w) = -\frac{f_{cap\,(w)}}{\alpha^{ss}}\frac{w}{w_s}\left[\left(\frac{w}{w_s}\right)^{n^{ss}/1-n^{ss}} - 1\right]^{1/n^{ss}} = -f_{cap\,(w)}\psi\left[1 + (\alpha^{ss}\psi)^{n^{ss}}\right]^{\frac{1}{n^{ss}}-1} \quad \textbf{(4- 5)}$$

$$f_{cap}(w) = \frac{1}{2}\left[1 + \operatorname{erf}\left(4\frac{w - w^{ss}_{tran}}{w^{ss}_{tran}}\right)\right] \quad \textbf{(4- 6)}$$

where $\sigma_{tu}(w)$ is uniaxial tensile strength, $\sigma_{tia}(w)$ is isotropic tensile strength, $\phi$ is soil friction angle, $\sigma^{s}_{ads}(w)$ is adsorptive suction stress, $f_{ads}(w)$ is a dimensionless scaling function reflecting the distribution of physicochemical forces in terms of probability, $\sigma^{s}_{dry}$ is suction stress at the oven-dry state, $\beta'$ is a dimensionless parameter reflecting the strength of adsorptive suction stress which determines the transition between adsorption and capillarity ($\beta'$ was suggested to be 4.0 for low-expansive and non-expansive soils and 2.0 for expansive and high-expansive soils) (Zhang and Lu 2020), $w^{ss}_{tran}$ represents the water content where adsorption water regime

transitions to capillary water regime (the range of $w_{tran}^{ss}$ changes from 0 for clean sands to as high as 0.35 for expansive clays) (Zhang and Lu 2020), $w_s$ is saturated gravimetric water content, $\sigma_{cap}^{s}(w)$ is capillary suction stress, $\psi$ is matric suction in kPa, $\alpha^{ss}$ is a fitting parameter related to the inverse of the average capillary suction stress depending mainly on the average pore size, soil type and void ratio (the larger the pore sizes, the higher $\alpha^{ss}$ values), $n^{ss}$ is a fitting parameter related to the pore-size distribution for the capillary suction stress controlling the slope of the capillary suction stress between the transitional water and saturated water content (the range of $n^{ss}$ changes from 1.5 to 3) (Zhang and Lu 2020).

To develop a temperature-dependent TSCC model, one needs to extend the isothermal isotropic tensile strength $\sigma_{tia}(w)$ to temperature-dependent conditions ($\sigma_{tia}(w,T)$) by incorporating the effects of temperature, $T$, into the parameters contributing to Eq. (2). The following sections present the temperature-dependent extension of the adsorptive and capillary suction stresses.

### 4.3 Temperature-Dependent Adsorptive Suction Stress

Adsorptive suction stress is defined as the maximum adsorptive suction $\sigma_{dry}^{s}$ stress multiplied by a dimensionless scaling function $f_{ads}(w)$. Assuming the controlling role of van der Waals forces in controlling adsorbed water film thickness, Tuller and Or (2005) provided a relationship between water content and matric suction at the dry end (low range of water contents) as follows:

$$w = \sqrt[3]{\frac{A_{svl}}{6\pi\psi}} SA\rho_w \qquad \textbf{(4- 7)}$$

where $w$ is gravimetric water content, $A_{svl}$ is the Hamaker constant, $\rho_w$ is the density of water (998.23 kg/m$^3$), and SA is specific surface area in m$^2$/kg. Note that Eq. (7) is developed for specific surface areas smaller than 200 m$^2$/g. SA is a soil property that can be experimentally measured in the laboratory. Solving Eq. (7) for $\psi$ yields a soil water retention curve (SWRC) model at the dry end as follows:

$$\psi = \frac{A_{svl}{\rho_w}^3 SA^3}{6\pi w^3} \qquad \textbf{(4- 8)}$$

Lu et al. (2010) defined suction stress $\sigma^s$ under ambient temperature as:

$$\sigma^s = -(S_e\psi)_{T_r} \qquad \textbf{(4- 9)}$$

where $S_e$ is effective degree of saturation at an arbitrary reference temperature ($T_r$) and can be defined as:

$$S_e = \frac{w - w_{tran}^{ss}}{ws - w_{tran}^{ss}} \quad \textbf{(4- 10)}$$

Note that other expressions for suction stress are proposed in the literature (e.g. Alonso et al. 2010). Incorporating Eqs. (8 and 10) into Eq. (9) leads to the following equation for suction stress at the dry end where adsorption is prominent:

$$\sigma^s = -\frac{A_{svl}{\rho_w}^3 SA^3}{6\pi w^2}\frac{w - w_{tran}^{ss}}{ws - w_{tran}^{ss}} \quad \textbf{(4- 11)}$$

Eq. (11) can be reduced to Eq. (12) to determine the maximum adsorptive suction $\sigma_{dry}^{s}$ when water content reaches to the adsorption strength ($w_{amax}$) that accounts for adsorptive water:

$$\sigma_{dry}^{s} = -\frac{A_{svl}{\rho_w}^3 SA^3}{6\pi w_{amax}^2}\frac{w_{amax} - w_{tran}^{ss}}{ws - w_{tran}^{ss}} \quad \textbf{(4- 12)}$$

To extend Eq. (12) to temperature-dependent conditions, the temperature-dependent forms of the Hamaker constant $A_{svl}(T)$, water density $\rho_w(T)$, and surface area SA(T) need to be incorporated into Eq. (12). Israelachvili (2011) expressed the temperature-dependent Hamaker constant based on Lifshitz theory as follows:

$$A_{svl}(T) \approx \frac{3}{4}kT\left(\frac{\varepsilon_1-\varepsilon_3}{\varepsilon_1+\varepsilon_3}\right)\left(\frac{\varepsilon_2-\varepsilon_3}{\varepsilon_2+\varepsilon_3}\right) + \frac{3h}{4\pi}\int_{v_1}^{\infty}\left(\frac{\varepsilon_1(iv)-\varepsilon_3(iv)}{\varepsilon_1(iv)+\varepsilon_3(iv)}\right)\left(\frac{\varepsilon_2(iv)-\varepsilon_3(iv)}{\varepsilon_2(iv)+\varepsilon_3(iv)}\right)dv \quad \textbf{(4- 13)}$$

where $k$ is Boltzmann constant ($1.38 \times 10 - 23$ $m^2$ kg $s^{-2}$ $K^{-1}$), T is temperature in Kelvin, $\varepsilon_1$=80, $\varepsilon_2$=25, and $\varepsilon_3$=1 are the static dielectric constants of clay, water, and air, respectively, $h$ is the Plank constant, $v$ is the orbiting frequency of electrons, $\varepsilon\ (iv)$ are the values of $\varepsilon$ at imaginary frequencies. Tuller and Or (2005) found that Eq. (11) is in an excellent agreement with laboratory-measured data using an effective Hamaker constant of $-6 \times 10^{-20}$ J at ambient temperature.

This statement and substituting the $\varepsilon_1$, $\varepsilon_2$, and $\varepsilon_3$ values convert Eq. (13) into the following equation for soils:

$$A_{svl}(T) = 0.675kT + 5.73 \times 10^{-20} \quad \textbf{(4- 14)}$$

Density of water can be written as a function of temperature as follows:

$$\rho_w(T) = \frac{\rho_{W(T=293K)}}{1 + \alpha(T - 293)} \quad \textbf{(4- 15)}$$

where $\alpha$ is the coefficient of volume expansion of water ($-210 \times 10^{-6}\ 1/℃$). The thermal volume expansion of the pore water in clays has been shown to be dependent on temperature and effective stress, and to be different from the one of pure water (Baldi et al. 1988). The influence of temperature becomes profound in cases of high effective stresses and temperatures higher than 60℃. For the range of temperatures examined in this study (from 20 $to$ 60℃ ), we assume $\alpha$ to be constant.

Experimental studies on the impact of elevated temperatures on soil specific surface area have revealed that this component does not change dramatically with changes in temperature less than 100℃ (Goodman and Vahedifard 2019). In this study, the authors assume that SA remains constant within the range of temperatures examined (from 20 $to$ 60℃ ). The full expression for the temperature-dependent adsorptive suction stress is:

$$\sigma^s_{ads}(w,T) = -\frac{A_{svl}(T)\rho_w(T)^3 SA^3}{6\pi w^2_{amax}} \frac{w_{amax} - w^{ss}_{tran}}{ws - w^{ss}_{tran}} f_{ads}(w) \quad \textbf{(4- 16)}$$

### 4.4 Temperature-Dependent Capillary Suction Stress

Following the procedure outlined in Vahedifard et al. (2018b, 2019), the temperature-dependent capillary suction stress is derived by incorporating thermal induced changes in surface tension, contact angle and enthalpy of immersion. The temperature-dependent version of Eq. (5) is:

$$\sigma_{cap}^{s}(w,T) = -f_{cap\ (w)}\psi(w,T)\left[1 + (\alpha^{ss}\psi(w,T))^{n^{ss}}\right]^{\frac{1}{n^{ss}}-1} \quad \textbf{(4- 17)}$$

Grant and Salehzadeh (1996) expressed the temperature dependency of capillary pressure as:

$$\psi(w,T) = \psi_{T_r}\left(\frac{\beta + T}{\beta_{T_r} + T_r}\right) \quad \textbf{(4- 18)}$$

where $\psi_{T_r}$ is the capillary pressure at the reference temperature of $T_r$, $\beta_{T_r}$ is a regression parameter at the reference temperature; $\beta$ is calculated as (Grant and Salehzadeh 1996):

$$\beta = \frac{-\Delta h}{C_1} \quad \textbf{(4- 19)}$$

where $\Delta h$ is the enthalpy of immersion per unit area, $C_1$ is a constant determined through the following equation (Grant and Salehzadeh 1996):

$$C_1 = \frac{\Delta \mathrm{h}_{T_r} + \sigma\, cos\alpha}{T_r} \quad \textbf{(4- 20)}$$

where $\alpha$ is the temperature-dependent soil-water contact angle, $\Delta \mathrm{h}_{T_r}$ is the enthalpy of immersion per unit area at $T_r$, $\sigma$ is water-air surface tension, which can be described as follows (Haar 1984; Dorsey 1940):

$$\sigma = a' + b\,T \tag{4- 21}$$

where $a'$ and $b$ are fitting parameters that can be estimated as (Haar 1984; Dorsey 1940):

$$a' = 0.11766 \pm 0.00045\ Nm^{-1}$$
$$b = -0.0001535 \pm 0.0000015\ Nm^{-1}K^{-1} \tag{4- 22}$$

Watson (1943) expressed the temperature dependency of the enthalpy immersion as follows:

$$\Delta h = \Delta h_{T_r}(\frac{1 - T_r}{1 - T})^{0.38} \tag{4- 23}$$

where $\Delta h_{T_r}$ is the enthalpy immersion per unit area at the reference temperature. Vahedifard et al. (2018b) expressed the temperature-dependent contact angle as:

$$cos\alpha = \frac{-\Delta h + TC_1}{a + bT} \tag{4- 24}$$

Finally, one can obtain the uniaxial tensile strength model under elevated temperatures as follows:

$$\sigma_{tu}(w,T) = 2\sigma_{tia}(w,T)\tan\phi\tan\left(\frac{\pi}{2} - \frac{\phi}{4}\right) \tag{4- 25}$$

$$\sigma_{tia}(w) = \sigma^s_{ads}(w,T) + \sigma^s_{cap}(w,T) \tag{4- 26}$$

### 4.5 Validation and Comparison

The proposed TSCC model is validated against experimentally measured tensile strength data reported by Salimi et al. (2021a) for two clays including a highly plastic clay (Idabel Clay) and a medium plastic clay (Chickasha Clay). Salimi et al. (2021a) used a desiccation test apparatus and directly measured the tensile strength of the clays during desiccation at 20, 40, and 60°C. For each soil, the validation process included two steps: (a) we first calibrated the model at ambient temperature (20°C) to determine the fitting parameters yielding the minimum error compared to measured values, and (b) we then employed the calibrated model to predict the tensile strength for each clay at elevated temperatures (40 and 60°C) and compared the predicted values against laboratory-measured results. Table 4. 1 shows the measured geotechnical parameters for Idabel and Chickasha clays. The SSCC parameters for these clays were deduced based on the suggestions made by Zhang and Lu (2020), listed in Table 4. 2. A key advantage of the proposed TSCC model is that the formulation only requires one additional parameter, $\Delta \mathrm{h}_{T_r}$, to account for the effect of temperature. Measured $\Delta h_{T_r}$ values for different soil types are presented by Grant and Salehzadeh (1996) and Vahedifard et al. (2020). In this study, $\Delta \mathrm{h}_{T_r}$= -516 mJ/m$^3$ is used for both soils, consistent with the values reported by Grant and Salehzadeh (1996) for comparable soils.

Lu (2016) presented a SWRC model that separately accounts for capillarity and adsorption water contents. The Lu (2016) SWRC model can be rewritten using gravimetric water content as follows:

$$w = w_a + w_c \tag{4- 27}$$

$$w_a = w_{amax}\left\{1 - \left[\exp\left(\frac{\psi - \psi_{max}}{\psi}\right)\right]^{1/n^{ss}}\right\} \quad \textbf{(4- 28)}$$

$$w_c = (w_s - w_a)\left[1 + (\alpha^{ss}\psi)^{n^{ss}}\right]^{-1/n^{ss}} \quad \textbf{(4- 29)}$$

where $w_a$ is the adsorptive gravimetric water content, $w_c$ is the capillary gravimetric water content; $w_{amax}$ is the adsorption strength, $\psi_{max}$ is the matric suction corresponding to the adsorption strength.

The Lu (2016) SWRC model (Eqs. 27-29) can be extended to incorporate the effect of temperature if suction $\psi$ is extended to the temperature-dependent suction $\psi(w, T)$ (Eq. 18) as:

$$w_a = w_{amax}\left\{1 - \left[\exp\left(\frac{\psi(w,T) - \psi_{max}(w,T)}{\psi(w,T)}\right)\right]^{1/n^{ss}}\right\} \quad \textbf{(4- 30)}$$

$$w_c = (w_s - w_a)\left[1 + (\alpha^{ss}\psi(w,T))^{n^{ss}}\right]^{-1/n^{ss}} \quad \textbf{(4- 31)}$$

Figs. 4. (1 and 2) show the SWRCs and the SSCCs for Idabel Clay (Figs. 4. (1a and 2a)) and Chickasha Clay (Figs. 4. (1b and 2b)) at different temperatures, respectively. The soil water retention mechanism of soils changes under elevated temperatures since high temperature change the surface tension of the pore water, soil-water contact angle, soil fabric, water absorption potential, pore size distribution of soils, and enthalpy (e.g., Grant and Salehzadeh 1996; Romero et al. 2003; Wan et al. 2015; Vahedifard et al. 2018b). These changes result in a reduction in capillary and adsorptive water, primarily in the capillary water, as shown in Figs. 4. (1 and 2).

Fig. 4. 3 provides a comparison between measured and predicted tensile strengths for Idabel Clay (Fig. 4. 3a) and Chickasha Clay (Fig. 4. 3b) at temperatures of 20, 40, and 60 °C. The accuracy of

the model for each soil is examined by calculating the coefficient of determination ($R^2$) and the root mean square error (RMSE) between the predicted and measured data.

At a given water content, the measured data in Fig. 4. 3 show that the tensile strength decreases as temperature elevates. The effect of temperature is more pronounced for the low matric suctions when capillarity is the governing mechanism in the development of tensile strength. For example, at a water content of 20% (suction= 40 kPa), a 40% reduction in tensile strength of Chickasha clay is observed when temperature increases from 20 °C to 60 °C (Fig. 4. 4b). The apparent cohesion caused by capillary water weakens under high temperatures resulting in a reduction in the tensile strength. High temperatures indeed reduce the surface tension; expand the trapped air bubbles; isolate water packets; and change the quality of solute (Romero and Simms 2008; Schneider and Goss 2011). In contrast, elevated temperatures have almost no impact on tensile strength when adsorption mechanism is dominant. Adsorptive water is mostly trapped in intra-aggregate pores (micropores) due to attractive van der Waals forces and electrostatic repulsion forces. The temperature has the least influence on the dominant van der Waals forces because they are due to electronic fluctuations. As evident from the $R^2$ and RMSE values shown in Fig. 4. 3, the proposed TSCC model accurately captures the laboratory-measured tensile strength values for both clays at different temperatures.

**Table 4. 1. Measured parameters of soils used for model validation and comparison.**

| Soil | USCS | Void ratio | $SA$ ($m^2/g$) | LL (%) | PL (%) | PI | Specific gravity | $\emptyset'$ (deg.) | $w_s$ (g/g) |
|---|---|---|---|---|---|---|---|---|---|
| Idabel clay | CH | 1.07 | 145.5 | 72 | 26 | 46 | 2.78 | 15.6 | 0.385 |
| Chickasha clay | CL | 0.66 | 107.5 | 38 | 20 | 18 | 2.57 | 29.0 | 0.257 |

**Table 4. 2. Input parameters for the SSCC and TSCC**

| soils | Fitted parameters | | | Assumed parameters | |
|---|---|---|---|---|---|
| | $\alpha^{ss}$ ($kPa^{-1}$) | $n^{ss}$ | $\beta$ | $w_{tran}^{ss}$ (g/g) | $w_{a\,max}$ (g/g) |
| Idabel clay | 0.008 | 2 | 2 | 0.19 | 0.06 |
| Chickasha clay | 0.020 | 2 | 2 | 0.13 | 0.059 |

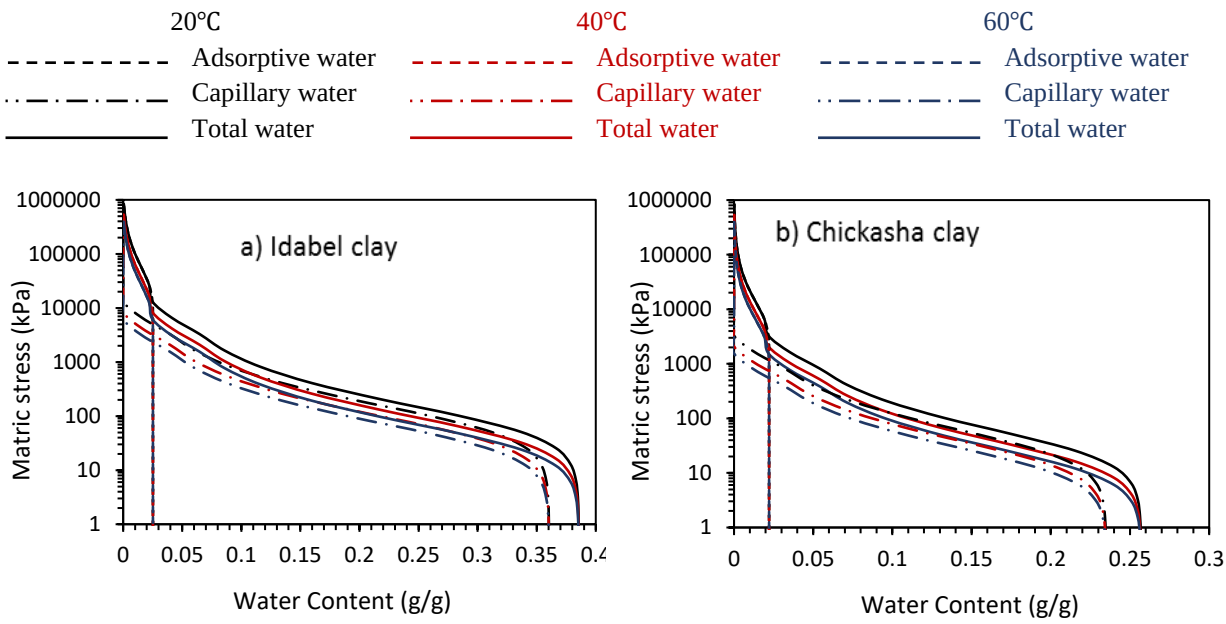



**Figure 4. 1. Soil water retention curve (SWRC) at different temperatures (a) Idabel Clay; (b) Chickasha Clay.**

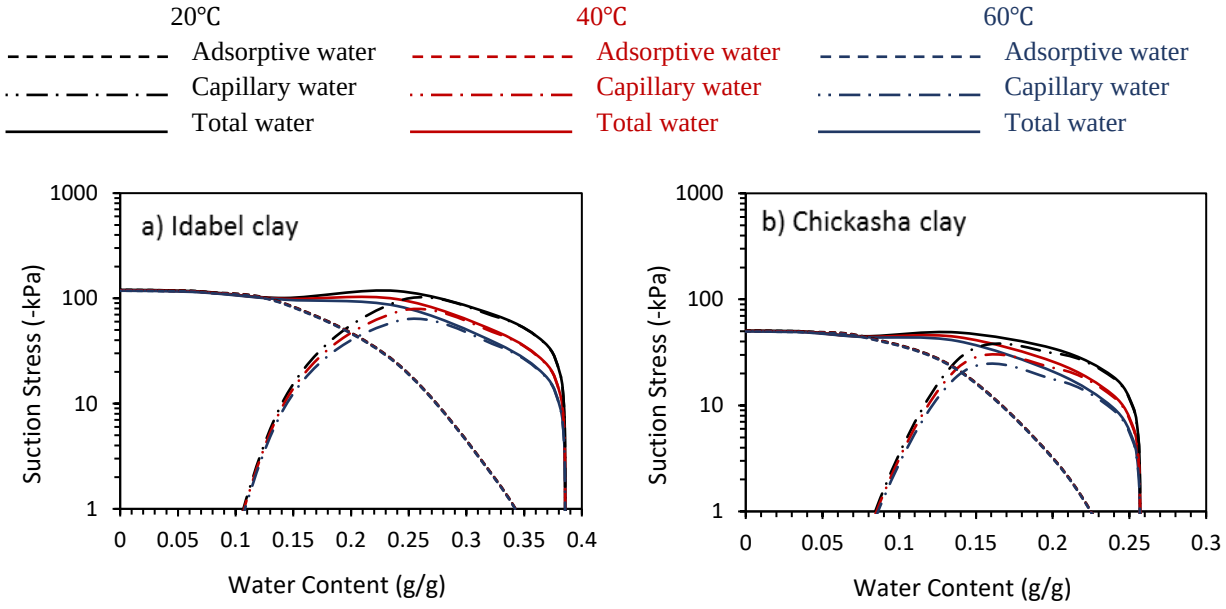



**Figure 4. 2. Suction stress characteristic curve (SSCC) at different temperatures: (a) Idabel Clay; (b) Chickasha Clay.**

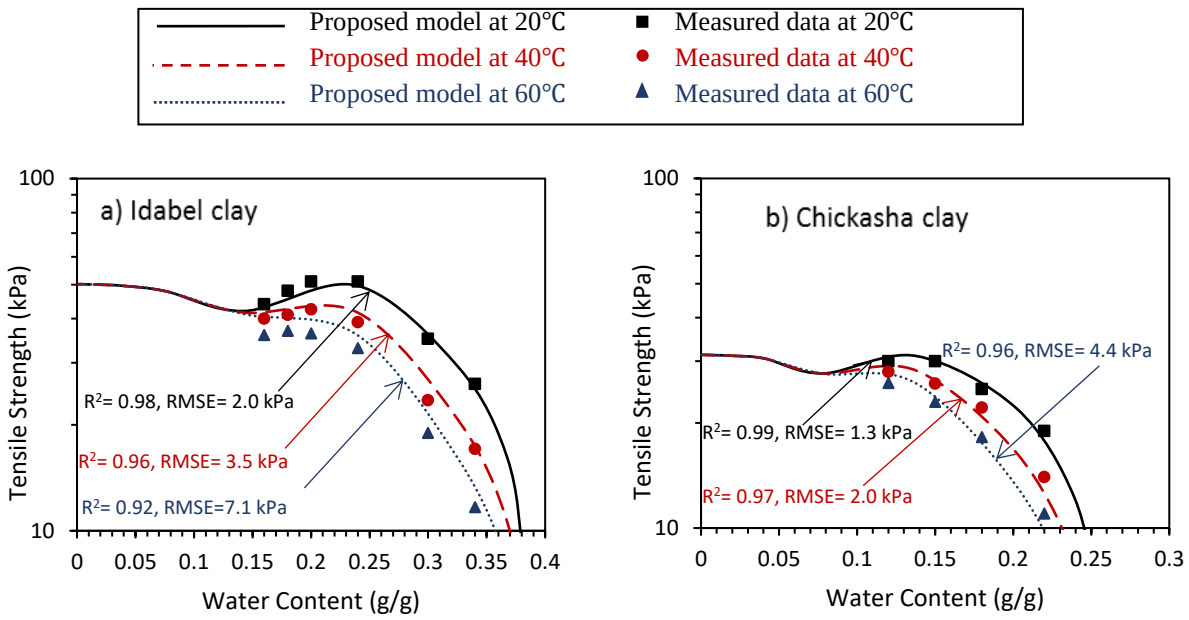



**Figure 4. 3. Tensile strength characteristic curve (TSCC) at different temperatures: (a) Idabel Clay; (b) Chickasha Clay.**

The proposed TSCC model in this study offers a generalized framework to determine the tensile strength of unsaturated soils while accounting for the effect of temperature. The proposed model can be readily employed in a wide range of geotechnical and geoenvironmental engineering applications where the tensile strength of unsaturated soils is needed. Elevated temperatures mean different values for different applications. For instance, under climatic interactions, the surface temperature can reach a maximum value of around 50°C. In several near-surface geo-energy applications (e.g., energy piles, thermally active earthen systems, energy tunnels, energy diaphragm walls, energy sheet piles), the maximum temperature posed to the soil is generally limited to about 60°C. In this paper, we validated the proposed TSCC model with laboratory-measured data up to 60°C, which covers the maximum temperature involved in several of the aforementioned applications.

# CHAPTER 5: CONCLUSIONS AND RECOMMENDATIONS

## 5.1 Summary and Conclusion: Tensile Strength of Compacted Clays during Desiccation under Elevated Temperatures

Several processes leading to the formation of cracks in unsaturated soils as well as several critical engineering applications subject unsaturated soils to elevated temperatures. Thus, it is essential to enhance the state of the knowledge regarding the behavior of unsaturated soils under elevated temperatures. Tensile strength is a key parameter to properly analyze the onset and propagation of desiccation cracks in slopes and earth structures.

A direct desiccation-tensile test apparatus was used to investigate the tensile strength of unsaturated soils under elevated temperature conditions. A series of direct tensile tests were carried out on remolded specimens of two clayey soils with low to high plasticity compacted over a range of water contents. The effect of compaction water content, elevated temperature ranging from 20 °C to 60 °C, and soil type on the development of the tensile strength of the tested clays were analyzed and discussed. The experimental data for tensile strength of unsaturated soils under elevated temperature conditions was presented, which were the first data set of its kind to be published in the literature. These data are necessary for development and validation purpose of modeling efforts in future studies. Specific conclusions gleaned from this research include:

1. Elevated temperatures affect the tensile strength.
2. The tensile strength of the clays decreased when the drying temperature increased from 20 °C to 60 °C.

3. The initial water content from dry to wet of optimum had a significant effect on the development of the tensile strength in both soils.
4. Tensile strength increased with increasing the water content to a peak value and then decreased afterward.
5. Clays with higher plasticity index exhibited greater tensile strength.

## 5.2 Summary and Conclusions: Tensile Strength of Compacted Clays during Desiccation under Elevated Temperatures

It is essential to predict the tensile strength of unsaturated soils in order to study the influence of tensile and desiccation cracks on slopes and earthen structures because the initiation and propagation of cracks are directly related to tensile strength. There is no unified tensile strength model that can capture tensile strength of variety of unsaturated soils ranging from clean sands to silty and clayey soils over the entire range of water content and. A general model for tensile strength characteristic curve was presented that can reasonably predict the tensile strength of a variety of unsaturated soils ranging from clean sands to silty and clayey soils. The model was built by separately considering the effects of adsorptive and capillary soil water interaction mechanisms on the development of the interparticle forces and the resultant tensile strength. A two-part suction stress characteristic curve was used as a tool to predict the tensile strength because suction stress combines both the capillary and adsorptive stresses. Laboratory measured tensile strength for ten different soils reported in the literature were then used to validate the

predictive accuracy of the proposed model to compare against four alterative models. Specific conclusions from this portion of the research are as follows:

1. The changes in water content affected the development of tensile strength.
2. The tensile behavior of compacted sandy soils was different from fine-grained soils.
3. Tensile strength vanished at both the dry and fully saturated conditions for sands, while a noticeable tensile strength was observed when clayey soils were dry.
4. The findings of this study emphasize that the adsorptive interparticle forces play a major role in the development of tensile strength in compacted fine-grained soils.
5. A better understanding of the tensile strength will help us to determine the depth of desiccation cracks more accurately in earthen structures such as embankments, dams, slopes, and hydraulic barriers. As a result, a more realistic stability analysis can be conducted.

## 5.3 Summary and Conclusion: A General Model for the Uniaxial Tensile Strength Characteristic Curve of Unsaturated Soils

Tensile strength is a key parameter controlling the formation of desiccation cracks in soils. Desiccation cracks are triggered in unsaturated soils due to drying imposed by natural processes or engineering applications mainly involving elevated temperatures. A temperature-dependent model for the tensile strength characteristic curve of unsaturated soils was presented and validated by laboratory measured tensile strength of two clay soils at temperatures of 20, 40, and 60 °C. The model was built by employing suction stress and incorporating the effects of

temperature into adsorptive and capillary suction stress components. The temperature-dependent adsorptive suction stress was obtained by accounting for thermal induced changes in suction stress at dry state through the Hamaker constant and the density of water. The temperature-dependent form of capillary suction stress was derived by employing temperature-dependent forms of surface tension, contact angle and enthalpy of immersion. The temperature-dependent model for the tensile strength characteristic curve of unsaturated soils can be integrated into analytical and numerical simulations leading to more accurate assessment of desiccation cracking in unsaturated slopes and earthen structures subject to elevated temperatures. Specific conclusions that can be extracted from this section of the research are:

- The model can seamlessly estimate the tensile strength of unsaturated soils at given water content and temperature spanning capillary and adsorptive water retention mechanisms.
- The thermal effect on the tensile strength component attributed to the capillarity mechanism was found to be significant, whereas the effect on the adsorptive component of the tensile strength was insignificant.
- The model can be readily employed to represent the tensile strength in analytical and numerical analyses of desiccation cracking in unsaturated slopes and earthen structures subject to varying water content and temperature.

## 5.4 Summary and Conclusion: A Temperature-Dependent Model for Tensile Strength Characteristic Curve of Unsaturated Soils

Tensile strength is a key parameter controlling the formation of desiccation cracks in soils. Desiccation cracks are triggered in unsaturated soils due to drying imposed by natural processes or engineering applications mainly involving elevated temperatures. A temperature-dependent model for the tensile strength characteristic curve of unsaturated soils was presented and validated by laboratory measured tensile strength of two clay soils at temperatures of 20, 40, and 60 °C. The model was built by employing suction stress and incorporating the effects of temperature into adsorptive and capillary suction stress components. The temperature-dependent adsorptive suction stress was obtained by accounting for thermal induced changes in suction stress at dry state through the Hamaker constant and the density of water. The temperature-dependent form of capillary suction stress was derived by employing temperature-dependent forms of surface tension, contact angle and enthalpy of immersion. The temperature-dependent model for the tensile strength characteristic curve of unsaturated soils can be integrated into analytical and numerical simulations leading to more accurate assessment of desiccation cracking in unsaturated slopes and earthen structures subject to elevated temperatures.

**5.5 Recommendations:**

1. More Experimental tests are suggested to further verify the proposed temperature-dependent tensile strength model over a wider range of temperatures and soils. It is suggested to measure suction for each soil at elevated temperatures.
2. It is suggested to measure crack depths at elevated temperatures under controlled laboratory conditions for a wide range of soils and temperatures.
3. It is suggested to establish a novel constitutive model for characterization of crack depth using the general proposed model for the uniaxial tensile strength characteristic curve of unsaturated soils.
4. A temperature-dependent framework for crack depth of unsaturated soils can be constructed based on the proposed temperature-dependent model for tensile strength characteristic curve of unsaturated soils.
5. The impact of crack depth and elevated temperatures on the integrity of energy geo-infrastructures should be investigated.
6. It is suggested to provide insights on the impact of desiccation cracks on the stability of tailing dams in changing temperature conditions.
7. It is suggested to perform case studies on soil deformation, lateral earth pressure, suction stress in different seasons when different temperatures is recorded for the validation purpose.

**REFERENCES**

Abbate, A., Longoni, L., Ivanov, V. I., & Papini, M. (2019). Wildfire impacts on slope stability triggering in mountain areas. *Geosciences, 9*(10), 417.

Ajaz, A., & Parry, R. (1975). Stress–strain behaviour of two compacted clays in tension and compression. *Geotechnique, 25*(3), 495-512.

Al-Hussaini, M. M., & Townsend, F. C. (1974). Investigation of tensile testing of compacted soils.

Albrecht, B. A., & Benson, C. H. (2001). Effect of desiccation on compacted natural clays. *Journal of Geotechnical and Geoenvironmental Engineering, 127*(1), 67-75.

Amarasiri, A., & Kodikara, J. (2011). Use of material interfaces in DEM to simulate soil fracture propagation in Mode I cracking. *International Journal of Geomechanics, 11*(4), 314-322.

Ávila, G. (2004). *Study on the cracking behaviour of clay. Application to Bogota clay.* Ph. D. thesis, Technical Univ. of Catalonia, Barcelona, Spain.

Ayad, R., Konrad, J.-M., & Soulié, M. (1997). Desiccation of a sensitive clay: application of the model CRACK. *Canadian Geotechnical Journal, 34*(6), 943-951.

Baldi, G., Hueckel, T., & Pellegrini, R. (1988). Thermal volume changes of the mineral–water system in low-porosity clay soils. *Canadian Geotechnical Journal, 25*(4), 807-825.

Barzegar, A., Oades, J., Rengasamy, P., & Murray, R. (1995). Tensile strength of dry, remoulded soils as affected by properties of the clay fraction. *Geoderma, 65*(1-2), 93-108.

Başer, T., Dong, Y., Moradi, A., Lu, N., Smits, K., Ge, S., . . . McCartney, J. (2018). Role of nonequilibrium water vapor diffusion in thermal energy storage systems in the vadose zone. *Journal of Geotechnical and Geoenvironmental Engineering, 144*(7), 04018038.

Cannon, S. H., & Gartner, J. E. (2005). Wildfire-related debris flow from a hazards perspective *Debris-flow hazards and related phenomena* (pp. 363-385): Springer.

Cheng, Q., Tang, C.-S., Zeng, H., Zhu, C., An, N., & Shi, B. (2020). Effects of microstructure on desiccation cracking of a compacted soil. *Engineering Geology, 265*, 105418.

Coccia, C. J., Gupta, R., Morris, J., & McCartney, J. S. (2013). Municipal solid waste landfills as geothermal heat sources. *Renewable and sustainable energy reviews, 19*, 463-474.

Costa, S., Kodikara, J., & Shannon, B. (2013). Salient factors controlling desiccation cracking of clay in laboratory experiments. *Geotechnique, 63*(1), 18-29.

Cui, Y., Lu, Y., Delage, P., & Riffard, M. (2005). Field simulation of in situ water content and temperature changes due to ground–atmospheric interactions. *Geotechnique, 55*(7), 557-567.

Dorsey, N. E. (1940). Properties of ordinary water-substance in all its phases.

Ettala, M., Rahkonen, P., Rossi, E., Mangs, J., & Keski-Rahkonen, O. (1996). Landfill fires in Finland. *Waste Management & Research, 14*(4), 377-384.

Fang, H., & Fernandez, J. (1981). Determination of tensile strength of soils by unconfined-penetration test *Laboratory shear strength of soil*: ASTM International.

Fisher, R. (1926). On the capillary forces in an ideal soil; correction of formulae given by WB Haines. *The Journal of Agricultural Science, 16*(3), 492-505.

Garrido, C., Otero, A. F., & Cidras, J. (2003). Theoretical model to calculate steady-state and transient ampacity and temperature in buried cables. *IEEE transactions on power delivery, 18*(3), 667-678.

Ghosh, A., & Subbarao, C. (2006). Tensile strength bearing ratio and slake durability of class F fly ash stabilized with lime and gypsum. *Journal of Materials in Civil Engineering, 18*(1), 18-27.

Goodman, C., & Vahedifard, F. (2019). Micro-scale characterisation of clay at elevated temperatures. *Géotechnique Letters, 9*(3), 225-230.

Grant, S. A., & Salehzadeh, A. (1996). Calculation of temperature effects on wetting coefficients of porous solids and their capillary pressure functions. *Water Resources Research, 32*(2), 261-270.

Haar, L. (1984). *NBS/NRC steam tables*: CRC Press.

Haines, W. B. (1925). Studies in the physical properties of soils: II. A note on the cohesion developed by capillary forces in an ideal soil1. *The Journal of Agricultural Science, 15*(4), 529-535.

Ingles, O. (1962). Bonding forces in soils. Part 3. Theory of tensile strength for stabilised and naturally coherent soils.

Israelachvili, J. N. (2011). *Intermolecular and surface forces*: Academic press.

Kayyal, M. (1996). *Effect of the moisture evaporative stages on the development of shrinkage cracks in soils.* Paper presented at the Unsaturated soils.

Khan, M. S., Hossain, S., Ahmed, A., & Faysal, M. (2017). Investigation of a shallow slope failure on expansive clay in Texas. *Engineering Geology, 219*, 118-129.

Kim, T.-H., & Hwang, C. (2003). Modeling of tensile strength on moist granular earth material at low water content. *Engineering Geology, 69*(3-4), 233-244.

Kim, T.-H., Kim, T.-H., Kang, G.-C., & Ge, L. (2012). Factors influencing crack-induced tensile strength of compacted soil. *Journal of Materials in Civil Engineering, 24*(3), 315-320.

Kim, T., Kim, C., Jung, S., & Lee, J. (2007). Tensile strength characteristics of contaminated and compacted sand-bentonite mixtures. *Environmental geology, 52*(4), 653-661.

Kodikara, J., & Costa, S. (2013). Desiccation cracking in clayey soils: mechanisms and modelling *Multiphysical testing of soils and shales* (pp. 21-32): Springer.

Lachenbruch, A. H. (1961). Depth and spacing of tension cracks. *Journal of Geophysical Research, 66*(12), 4273-4292.

Lakshmikantha, M., Prat, P., & Ledesma, A. (2006). *An experimental study of cracking mechanisms in drying soils.* Paper presented at the 5th ICEG Environmental Geotechnics: Opportunities, Challenges and Responsibilities for Environmental Geotechnics: Proceedings of the ISSMGE's fifth international congress organized by the Geoenvironmental Research Centre, Cardiff University and held at Cardiff City Hall on 26–30th June 2006.

Lakshmikantha, M., Prat, P. C., & Ledesma, A. (2012). Experimental evidence of size effect in soil cracking. *Canadian Geotechnical Journal, 49*(3), 264-284.

Li, H.-D., Tang, C.-S., Cheng, Q., Li, S.-J., Gong, X.-P., & Shi, B. (2019). Tensile strength of clayey soil and the strain analysis based on image processing techniques. *Engineering Geology, 253*, 137-148.

Lu, N. (2016). Generalized soil water retention equation for adsorption and capillarity. *Journal of Geotechnical and Geoenvironmental Engineering, 142*(10), 04016051.

Lu, N., Kim, T.-H., Sture, S., & Likos, W. J. (2009). Tensile strength of unsaturated sand. *Journal of engineering mechanics, 135*(12), 1410-1419.

Lu, N., & Likos, W. J. (2006). Suction stress characteristic curve for unsaturated soil. *Journal of Geotechnical and Geoenvironmental Engineering, 132*(2), 131-142.

Lu, N., Wu, B., & Tan, C. (2005). *A tensile strength apparatus for cohesionless soils.* Paper presented at the Advanced experimental unsaturated soil mechanics EXPERUS 2005.

Lutenegger, A., & Rubin, A. (2008). Tensile strength of some compacted fine-grained soils. *Unsaturated Soils: Advances in Geo-Engineering; Toll, DG, Augarde, CE, Gallipoli, D., Wheeler, SJ, Eds*, 411-415.

Ma, C., & Hueckel, T. (1992). Stress and pore pressure in saturated clay subjected to heat from radioactive waste: a numerical simulation. *Canadian Geotechnical Journal, 29*(6), 1087-1094.

McCartney, J. S., Jafari, N. H., Hueckel, T., Sánchez, M., & Vahedifard, F. (2019). Emerging thermal issues in geotechnical engineering *Geotechnical fundamentals for addressing new world challenges* (pp. 275-317): Springer.

Miller, C. J., Mi, H., & Yesiller, N. (1998). Experimental analysis of desiccation crack propagation in clay liners 1. *JAWRA Journal of the American Water Resources Association, 34*(3), 677-686.

Moradi, A., Smits, K. M., Massey, J., Cihan, A., & McCartney, J. (2015). Impact of coupled heat transfer and water flow on soil borehole thermal energy storage (SBTES) systems: Experimental and modeling investigation. *Geothermics, 57*, 56-72.

Morovatdar, A., Ashtiani, R. S., Licon, C., Tirado, C., & Mahmoud, E. (2020). Novel framework for the quantification of pavement damages in the overload corridors. *Transportation Research Record, 2674*(8), 179-191.

Morovatdar, A., Ashtiani, R. S., & Licon Jr, C. (2020). *Development of a mechanistic framework to predict pavement service life using axle load spectra from Texas overload corridors.* Paper presented at the International Conference on Transportation and Development 2020.

Morovatdar, A., Palassi, M., & Ashtiani, R. S. (2020). Effect of pipe characteristics in umbrella arch method on controlling tunneling-induced settlements in soft grounds. *Journal of Rock Mechanics and Geotechnical Engineering, 12*(5), 984-1000.

Morovatdar, A., Palassi, M., & Beizaei, M. (2020). *Evaluation of the efficiency of the umbrella arch method in urban tunneling subjected to adjacent surcharge loads.* Paper presented at the Geo-Congress 2020: Engineering, Monitoring, and Management of Geotechnical Infrastructure.

Morris, P. H., Graham, J., & Williams, D. J. (1992). Cracking in drying soils. *Canadian Geotechnical Journal, 29*(2), 263-277.

Nahlawi, H., Chakrabarti, S., & Kodikara, J. (2004). A direct tensile strength testing method for unsaturated geomaterials. *Geotechnical Testing Journal, 27*(4), 356-361.

Nahlawi, H., & Kodikara, J. K. (2006). Laboratory experiments on desiccation cracking of thin soil layers. *Geotechnical & Geological Engineering, 24*(6), 1641-1664.

Omidi, G., Thomas, J., & Brown, K. (1996). Effect of desiccation cracking on the hydraulic conductivity of a compacted clay liner. *Water, Air, and Soil Pollution, 89*(1), 91-103.

Peron, H., Hueckel, T., Laloui, L., & Hu, L. (2009). Fundamentals of desiccation cracking of fine-grained soils: experimental characterisation and mechanisms identification. *Canadian Geotechnical Journal, 46*(10), 1177-1201.

Prat, P. C., Ledesma, A., & Lakshmikantha, M. (2006). Size effect in the cracking of drying soil *Fracture of Nano and Engineering Materials and Structures* (pp. 1373-1374): Springer.

Robinson, J. D., & Vahedifard, F. (2016). Weakening mechanisms imposed on California's levees under multiyear extreme drought. *Climatic change, 137*(1), 1-14.

Rodríguez, R., Sanchez, M., Ledesma, A., & Lloret, A. (2007). Experimental and numerical analysis of desiccation of a mining waste. *Canadian Geotechnical Journal, 44*(6), 644-658.

Romero, E., Gens, A., & Lloret, A. (2001). Temperature effects on the hydraulic behaviour of an unsaturated clay *Unsaturated soil concepts and their application in geotechnical practice* (pp. 311-332): Springer.

Romero, E., Gens, A., & Lloret, A. (2003). Suction effects on a compacted clay under non-isothermal conditions. *Geotechnique, 53*(1), 65-81.

Romero, E., & Simms, P. H. (2008). Microstructure investigation in unsaturated soils: a review with special attention to contribution of mercury intrusion porosimetry and environmental scanning electron microscopy. *Geotechnical and Geological engineering, 26*(6), 705-727.

Rumpf, H. (1970). Zur theorie der zugfestigkeit von agglomeraten bei kraftuebertragung an kontaktpunkten. *Chemie Ingenieur Technik, 42*(8), 538-540.

Salata, F., Nardecchia, F., de Lieto Vollaro, A., & Gugliermetti, F. (2015). Underground electric cables a correct evaluation of the soil thermal resistance. *Applied Thermal Engineering, 78*, 268-277.

Salimi, K., Cerato, A. B., Vahedifard, F., & Miller, G. A. (2021). Tensile Strength of Compacted Clays during Desiccation under Elevated Temperatures. *Geotechnical Testing Journal, 44*(4).

Sánchez, M., Manzoli, O. L., & Guimarães, L. J. (2014). Modeling 3-D desiccation soil crack networks using a mesh fragmentation technique. *Computers and Geotechnics, 62*, 27-39.

Santamarina, J. C. (2003). Soil behavior at the microscale: particle forces *Soil behavior and soft ground construction* (pp. 25-56).

Schneider, M., & Goss, K. U. (2011). Temperature dependence of the water retention curve for dry soils. *Water Resources Research, 47*(3).

Senior, R. B. (1981). Tensile strength, tension cracks, and stability of slopes. *Soils and foundations, 21*(2), 1-17.

Stewart, M. A., Coccia, C. J., & McCartney, J. S. (2014). *Issues in the implementation of sustainable heat exchange technologies in reinforced, unsaturated soil structures.* Paper presented at the Geo-Congress 2014: Geo-characterization and Modeling for Sustainability.

Switzer, C., Zihms, S., & Tarantino, A. (2015). Effects of high temperatures on soil properties: Lessons to share from smouldering remediation experience. *Flamma, 6*(1), 5-7.

Take, W. A. (2003). *The influence of seasonal moisture cycles on clay slopes.* University of Cambridge.

Tamrakar, S. B., Toyosawa, Y., Mitachi, T., & Itoh, K. (2005). Tensile strength of compacted and saturated soils using newly developed tensile strength measuring apparatus. *Soils and foundations, 45*(6), 103-110.

Tang, A.-M., & Cui, Y.-J. (2005). Controlling suction by the vapour equilibrium technique at different temperatures and its application in determining the water retention properties of MX80 clay. *Canadian Geotechnical Journal, 42*(1), 287-296.

Tang, C.-S., Cui, Y.-J., Tang, A.-M., & Shi, B. (2010). Experiment evidence on the temperature dependence of desiccation cracking behavior of clayey soils. *Engineering Geology, 114*(3-4), 261-266.

Tang, C.-S., Pei, X.-J., Wang, D.-Y., Shi, B., & Li, J. (2015). Tensile strength of compacted clayey soil. *Journal of Geotechnical and Geoenvironmental Engineering, 141*(4), 04014122.

Tang, C., Shi, B., Liu, C., Zhao, L., & Wang, B. (2008). Influencing factors of geometrical structure of surface shrinkage cracks in clayey soils. *Engineering Geology, 101*(3-4), 204-217.

Tang, G. X., & Graham, J. (2000). A method for testing tensile strength in unsaturated soils. *Geotechnical Testing Journal, 23*(3), 377-382.

Tarantino, A., Romero, E., & Cui, Y. J. (2005). *Advanced Experimental Unsaturated Soil Mechanics: Proceedings of the International Symposium on Advanced Experimental Unsaturated Soil Mechanics, Trento, Italy, 27-29 June 2005*: CRC Press.

Towner, G. (1987). The mechanics of cracking of drying clay. *Journal of Agricultural Engineering Research, 36*(2), 115-124.

Trabelsi, H., Jamei, M., Zenzri, H., & Olivella, S. (2012). Crack patterns in clayey soils: Experiments and modeling. *International Journal for Numerical and Analytical Methods in Geomechanics, 36*(11), 1410-1433.

Tuller, M., & Or, D. (2005). Water films and scaling of soil characteristic curves at low water contents. *Water Resources Research, 41*(9).

Vahedifard, F., AghaKouchak, A., & Robinson, J. D. (2015). Drought threatens California's levees. *Science, 349*(6250), 799-799.

Vahedifard, F., Cao, T. D., Ghazanfari, E., & Thota, S. K. (2019). Closed-form models for nonisothermal effective stress of unsaturated soils. *Journal of Geotechnical and Geoenvironmental Engineering, 145*(9), 04019053.

Vahedifard, F., Cao, T. D., Thota, S. K., & Ghazanfari, E. (2018). Nonisothermal models for soil–water retention curve. *Journal of Geotechnical and Geoenvironmental Engineering, 144*(9), 04018061.

Vahedifard, F., Robinson, J. D., & AghaKouchak, A. (2016). Can protracted drought undermine the structural integrity of California's earthen levees? *Journal of Geotechnical and Geoenvironmental Engineering, 142*(6), 02516001.

Vahedifard, F., Thota, S. K., Cao, T. D., Samarakoon, R. A., & McCartney, J. S. (2020). Temperature-Dependent Model for Small-Strain Shear Modulus of Unsaturated Soils. *Journal of Geotechnical and Geoenvironmental Engineering, 146*(12), 04020136.

Vahedifard, F., Williams, J. M., & AghaKouchak, A. (2018). Geotechnical engineering in the face of climate change: Role of multi-physics processes in partially saturated soils *IFCEE 2018* (pp. 353-364).

Varsei, M., Miller, G. A., & Hassanikhah, A. (2016). Novel approach to measuring tensile strength of compacted clayey soil during desiccation. *International Journal of Geomechanics, 16*(6), D4016011.

Vesga, L. F. (2009). Direct tensile-shear test (DTS) on unsaturated kaolinite clay. *Geotechnical Testing Journal, 32*(5), 397-409.

Villar, M., Martín, P., & Lloret, A. (2005). *Determination of water retention curves of two bentonites at high tenperature.* Paper presented at the Advanced experimental unsaturated soil mechanics EXPERUS 2005.

Villar, M. V., & Lloret, A. (2004). Influence of temperature on the hydro-mechanical behaviour of a compacted bentonite. *Applied Clay Science, 26*(1-4), 337-350.

Wan, M., Ye, W.-M., Chen, Y., Cui, Y.-J., & Wang, J. (2015). Influence of temperature on the water retention properties of compacted GMZ01 bentonite. *Environmental earth sciences, 73*(8), 4053-4061.

Wang, J.-J., Zhu, J.-G., Chiu, C., & Zhang, H. (2007). Experimental study on fracture toughness and tensile strength of a clay. *Engineering Geology, 94*(1-2), 65-75.

Wang, L.-L., Tang, C.-S., Shi, B., Cui, Y.-J., Zhang, G.-Q., & Hilary, I. (2018). Nucleation and propagation mechanisms of soil desiccation cracks. *Engineering Geology, 238*, 27-35.

Watson, K. (1943). Thermodynamics of the liquid state. *Industrial & Engineering Chemistry, 35*(4), 398-406.

Yin, P., & Vanapalli, S. K. (2018). Model for predicting tensile strength of unsaturated cohesionless soils. *Canadian Geotechnical Journal, 55*(9), 1313-1333.

Zeh, R., & Witt, K. (2005). *Suction-controlled tensile strength of compacted clays.* Paper presented at the PROCEEDINGS OF THE INTERNATIONAL CONFERENCE ON SOIL MECHANICS AND GEOTECHNICAL ENGINEERING.

Zeng, H., Tang, C.-s., Cheng, Q., Inyang, H. I., Rong, D.-z., Lin, L., & Shi, B. (2019). Coupling effects of interfacial friction and layer thickness on soil desiccation cracking behavior. *Engineering Geology, 260*, 105220.

Zhang, C., & Lu, N. (2020). Unified effective stress equation for soil. *Journal of engineering mechanics, 146*(2), 04019135.

Zheng, L., Rutqvist, J., Birkholzer, J. T., & Liu, H.-H. (2015). On the impact of temperatures up to 200 C in clay repositories with bentonite engineer barrier systems: A study with coupled thermal, hydrological, chemical, and mechanical modeling. *Engineering Geology, 197*, 278-295.

Zhu, L., Shen, T., Ma, R., Fan, D., Zhang, Y., & Zha, Y. (2020). Development of cracks in soil: An improved physical model. *Geoderma, 366*, 114258.